Geochemistry of Paleoproterozoic Gunflint Formation carbonate: implications for hydrosphere-atmosphere evolution

Philip Fralick, Noah Planavsky, Justin Burton, Ian Jarvis, W.D. Addison, T.J. Barrett, G.R. Brumpton

PII: S0301-9268(16)30123-1
DOI: http://dx.doi.org/10.1016/j.precamres.2016.12.014
Reference: PRECAM 4633

To appear in: *Precambrian Research*

Received Date: 8 May 2016
Revised Date: 28 November 2016
Accepted Date: 17 December 2016

Please cite this article as: P. Fralick, N. Planavsky, J. Burton, I. Jarvis, W.D. Addison, T.J. Barrett, G.R. Brumpton, Geochemistry of Paleoproterozoic Gunflint Formation carbonate: implications for hydrosphere-atmosphere evolution, *Precambrian Research* (2016), doi: http://dx.doi.org/10.1016/j.precamres.2016.12.014

Geochemistry of Paleoproterozoic Gunflint Formation carbonate: implications for hydrosphere-atmosphere evolution

Philip Fralick[1], Noah Planavsky[2], Justin Burton[1], Ian Jarvis[3], W.D. Addison[1], T.J. Barrett[4] and G.R. Brumpton[1]

[1]Department of Geology, Lakehead University, Thunder Bay, Ontario, Canada, P7B 5E1, philip.fralick@lakeheadu.ca

[2]Department of Geology and Geophysics, Yale University, New Haven, CT, USA, 06511

[3]School of Geography, Geology and the Environment, Kingston University, London, Kingston upon Thames, UK, KT1 2EE

[4]Ore Systems Consulting, 29 Toronto St. S., Markdale, Ontario, Canada, N0C 1H0

ABSTRACT

The ~1880 Ma Gunflint Formation has played a critical role in shaping our view of the evolution of the Precambrian biosphere and the redox state of Earth's early oceans. Herein we present a study of the petrology and geochemistry of calcic grainstones and stromatolitic limestones present at the very top of the Gunflint Formation and compare them with underlying ankeritic grainstones that dominate the shore-proximal portion of the basin. Meteoric calcite cements in the upper limestones formed prior to the unit being brecciated and/or buried by debris carried by the blast cloud from the 1850 Ma Sudbury impact event. The intraclastic grains and cements in the limestone are highly enriched in V, Cr, U and REEs, with REE patterns similar to those of modern groundwater. Cr isotopes have a distinctly positive signature in most samples indicating formation of oxidized, hexavalent Cr during subaerial weathering. These redox-sensitive metals were transported in oxygenated groundwater and precipitated where the fluid encountered reducing conditions. In contrast, the underlying ankeritic marine grainstones have REE patterns similar to those of some modern-day venting hydrothermal fluids and earliest Paleoproterozoic seawater. This work suggests that significant levels of oxygen existed in the atmosphere at the time, whereas, even shallow areas of the world ocean remained very oxygen-deficient. The contrast in redox state of anoxic shallow-marine water verses oxic groundwater was probably linked to strong sub-seafloor hydrothermal circulation and extensive upwelling onto shallow shelves, which could have sustained widespread marine anoxia. More broadly, our study highlights the importance of investigating and

understanding lateral geochemical gradients, and the flux rates that control them, in shallow paleomarine settings.

Keywords: Proterozoic atmosphere, Precambrian oxygen levels, Proterozoic carbonates, atmospheric evolution, Precambrian ocean chemistry

1. INTRODUCTION

The shift from an anoxic to an oxic ocean-atmosphere system was one of the most dramatic transitions in Earth's history (Holland, 2005). Earth's redox evolution progressively modified (either directly or indirectly) almost all major biogeochemical cycles and played an important role in dictating the types and abundances of ore deposits. Furthermore, there appear to be important links between redox state of the ocean-atmosphere and biological/ecosystem evolution. Therefore, it is not surprising that there has been extensive and sustained research over the last half century into how and when the Earth became oxygenated.

Much of our early understanding of Earth's redox evolution comes from ore deposits. Extensive detrital uraninite and pyrite placer accumulations have long been assumed to mark an essentially anoxic atmosphere (Roscoe, 1969; Holland, 2005). The deposition of large oxide-facies iron formations was traditionally viewed as evidence for an ocean-atmosphere system where oxygen was restricted to only shallow parts of the oceans (e.g. Cloud, 1972, 1973). Recent advances, notably the application of ^{33}S and ^{36}S rare sulfur

isotope measurements to track ozone formation, and a large increase in the number of high-precision dates from Precambrian sedimentary units, have improved our understanding of Earth's redox evolution. The sulfur isotope results confirm views developed from detrital pyrite and uraninite placers (e.g., Roscoe, 1969) that atmospheric oxygen began to increase from very low levels in the earliest Paleoproterozoic (ca. 2.4 Ga), which is often referred to as the Great Oxidation Event or "GOE" (e.g., Holland, 2005). Sulfur isotope studies (Johnston et al., 2006) also suggest that large iron formations in the late Paleoproterozoic formed under a somewhat oxygenated atmosphere. However, in contrast to the traditional view, multiple workers in recent years have suggested that Earth did not undergo a unidirectional oxygen rise after the GOE (e.g. Canfield, 2005; Frei et al., 2010; Planavsky et al., 2012; Partin et al., 2013).

In order to better understand redox history during the late Paleoproterozoic (1.9-1.8 Ga), we have undertaken an integrated geochemical and petrographic study of the Gunflint iron formation succession. Specifically, we have examined the behavior of a suite of redox-sensitive metals in carbonate-facies iron formation deposited in shallow-marine settings, and approximately coeval carbonate cements, which formed from ancient meteoric waters in subaerially exposed carbonate grainstones, stromatolites and a layer of debris from the Sudbury impact event. This approach allows tracking of oxygen levels in both the ocean and atmosphere, because meteoric fluids are assumed to have equilibrated with the atmosphere before precipitating the cements.

2. GEOLOGICAL SETTING

The Gunflint Formation was deposited at 1878±1 Ma (Fralick et al., 1998, 2002) on a storm-dominated, broad, presently south-facing, continental shelf (Pufahl and Fralick, 2004). In the past the Gunflint and overlying Rove Formations have been interpreted both as a foreland assemblage, with load-driven subsidence resulting from Penokean Orogeny thrusting in the south (Hoffman, 1987; Barovich et al., 1989, Klasner et al., 1991; Southwick and Morey, 1991; Morey and Southwick, 1995) and as an extensional basin formed on the continental margin (Kissin and Fralick, 1994; Hemming et al., 1995; Van Wyck and Johnson, 1997). The determination of the age of the Gunflint ended this controversy as the 1878 Ma age (Fralick et al., 1998, 2002) is older than the 1835 to 1865 Ma Penokean Orogeny (Sims et al., 1989) that was thought, by some, to have caused the basin to form. The approximately 1832 Ma (Addison et al., 2005) overlying, siliciclastic Rove Formation is the correct age to possibly have formed during tectonic loading in the south. However, orogeny in the south would have generated sediment entering the basin from that direction and study of cored drill-holes across the shelf (Poulton et al., 2010) shows only fining to the south of the delta-submarine fan system forming the Rove. There is no sediment delivery from the south, strongly indicating a subaerial landmass did not exist to the south of the shelf. Connectivity to the world ocean is emphasized by abundant tidal deposits in the basin (Ojakangas, 1983). Also, geochemical trends observed in the Gunflint and Rove Formations, and ascribed to changes in ocean chemistry (Poulton et al., 2004, 2010), are present in time correlative chemical sedimentary rocks on other continents (Rasmussen et al., 2012), necessitating connectivity of the water masses.

The Gunflint Formation forms a portion of the Animikie Group, which comprises: 1) a basal unit of conglomerates and sandstones, Kakabeka Conglomerate, that are sporadically present in the north and thicken southward; 2) a middle unit of chemical sedimentary rocks of the Gunflint, Biwabik and Cuyuna Formations; and 3) an upper unit of carbonaceous, pyritic shales and turbiditic sandstones of the Rove and Virginia Formations (Figures 1 and 2). Goodwin (1956, 1960) described the stratigraphy of the Gunflint Formation as consisting of a Lower member, an Upper member and a capping Limestone member. The Lower member represents a transgressive-regressive cycle culminating in subaerial exposure in the north approximately 50 m above the base of the Formation (Fralick and Barrett, 1995) (Figure 2). The Upper member records renewed transgression with superimposed shoaling-upwards cycles (Pufahl and Fralick, 2000, 2004). The capping Limestone member is the only limestone unit in the Animikie Basin, but has not been previously investigated in detail. The majority of sediment in the Gunflint Formation was initially deposited as chemical mud that was subsequently reworked by wave activity into sandy tempestite layers (Fralick, 1988; Pufahl and Fralick, 2004; a similar process for generating sand grains was reported by Simonson and Goode, 1989). Tidal reworking has also been recognized (Ojakangas, 1983). The Gunflint Formation consists mostly of chert, iron oxides and iron carbonates (Floran and Papike, 1975), with the iron carbonates forming an important component in near-shore areas of the northern portion of the basin (Fralick, 1988). Tuffaceous intervals and minor basalt are also present in the upper Gunflint (Hassler and Simonson, 1989; Goodwin, 1960; respectively).

An ejecta layer, formed by the Sudbury impact event (1850±1 Ma: Krogh et al., 1984), lies at the top of the Gunflint Formation (Addison et al., 2005, 2010) (Figure 2). It is laterally very variable in both lithology and thickness. In drill core, where it was first identified and described, the ejecta layer is about one meter thick, and consists of sand-sized debris, including a centimeter- to decimeter-thick zone of accretionary lapilli (Addison et al., 2005; Pufahl et al., 2007). In the northern-most portion of the basin, and sporadically elsewhere in the basin, the impact debris forms a probable base-surge conglomerate that is meters in thickness (Addison et al., 2008; Addison et al., 2010; Fralick et al., 2012). In apparently more complete sections, the impact debris consists of fractured rubble from underlying units overlain by cross-stratified accretionary lapilli. This is followed upward, above a sharp contact, by sand-sized sediment containing chaotic, angular blocks of underlying lithologies, all of which is capped by a graded sandy layer (Cannon et al, 2010; Fralick et al., 2012).

The Gunflint Formation is sharply overlain by carbonaceous, pyritic shales of the Rove Formation (ca. 1832 Ma: Kissin et al., 2003; Addison et al., 2005) (Figure 2). These shales dominate the stratigraphic column for 100 meters and then pass gradationally upwards into outbuilding prodeltaic, turbidite lobes, which paleocurrent studies (Morey, 1967, 1969) indicate were fed by sediment derived from the newly risen TransHudson Orogenic belt to the northwest (Meric and Fralick, 2005).

Major hiatuses are present between the 1878 Ma Gunflint grainstones and the 1850 Ma impact layer, and between this layer and the 1832 Ma Rove Formation. The Penokean Orogeny, which spans 1865 to 1835 Ma, deformed the southern part of the basin (Sims et al., 1989), with some thrust faults developing in the northern area (Hill and Smyk, 2005). The Penokean Orogeny was caused by compression along the southern margin of the craton and deformation of an existing arc terrain. This orogeny, or the Trans-Hudson Orogeny to the west, may have caused up-warping throughout the basin and forced a regression of the Gunflint Sea. The Gunflint Formation is strongly silicified immediately below this regression surface.

The Limestone member capping the Gunflint Formation lies directly above the silicified surface, but below the ejecta-debris layer (Figure 2). It is regionally extensive in the northernmost part of the basin but sporadically developed elsewhere (Goodwin, 1960). Where present, the Limestone member is commonly about one to five meters thick, and rests on silicified strata of the upper Gunflint Formation. In the present study we compare petrographic features and whole-rock major element, trace element and Cr isotope compositions of shallow-marine ankeritic carbonates of the Gunflint Formation with the calcitic carbonates of the overlying Limestone member, in order to ascertain the nature of the fluids from which the two carbonate assemblages precipitated and how we can use this information to constrain Earth's atmospheric evolution.

3. METHODS

Samples of fresh carbonate-bearing rock were obtained from surface outcrops and crushed to powder. Those from Areas 1, 2 and 3 contained almost exclusively calcite, quartz and chlorite; those from Area 4 were composed of ankerite and quartz. Samples were analyzed at three different laboratories. ICP-MS analyses for the rare earth elements in samples from Areas 1, 4A and 4B were performed at Kingston University under the supervision of I. Jarvis. Both whole-rock samples and extractions using five percent HCl were analyzed. The dilute HCl extractions verified that the REEs in the samples from Areas 1, 2 and 3 were overwhelmingly contained within the calcite cement and any readily soluble minerals associated with this phase. Those from Area 4 were predominantly in the ankerite. Thus, physical micro-sampling was not necessary. ICP-MS analyses for U and the rare earth elements in samples from areas 2, 3 and duplicate samples from 4A and B were performed at the Ontario Geological Survey's Geoscience Laboratories in Sudbury, Ontario. The accuracy and precision of selected samples analyzed at both of these laboratories were verified using the ICP-MS facilities at Lakehead University. BaO interference causing erroneous Eu values was tested by cross-plotting Ba vrs Eu/Eu* Even though Ba concentrations vary by almost two orders of magnitude no correlation was found with height of positive Eu anomalies. In fact most of the samples with large positive Eu anomalies also have the lowest concentrations of Ba. All samples were also analyzed for Al, Fe, Mn, P, Cr and V using ICP-AES at Lakehead University, under the supervision of P. Fralick. Standard sample preparation and analytical techniques were used for all ICP-MS analyses (Tomlinson, 1999; Burnham et al., 2002; Burnham and Schweyer, 2004) and ICP-AES analyses (Church, 1981; Thompson and Walsh, 1989). Standards and blanks were embedded in all runs and

duplicate analyses were performed on some samples. Precision and accuracy for duplicates and standards analyzed by ICP-AES and ICP-MS are better than ± 10 %. Lower limits of detection for elements of interest are: V=1 ppm, Cr=2 ppm, U=0.011 ppm, P=15 ppm; REEs range from 0.12 ppm for Ce to 0.002 ppm for Lu. Analytical results are given in the data depository. Not all samples analyzed for V, Cr and P using ICP-AES were analyzed for U and the REEs using ICP-MS.

Rare earth elements were normalized using post Archean Australian shale (Taylor and McLennan, 1985). Ce anomalies were calculated using the proxy Pr/Pr*, where Pr/Pr*=Pr/(.5Ce+.5Nd). The formula Ce/Ce*=Ce/(.5La+.5Pr) should not be used when computing Ce anomalies for Paleoproterozoic and Archean chemical sediments as La is commonly anomalous in these rocks. This will lead to false Ce anomalies (Bau and Dulski, 1996). After Bau and Dulski (1996) put the use of Pr/Pr* forward as a proxy for calculating Ce anomalies in Precambrian chemical sediments its use became preferred (see: Kamber and Webb, 2001; Bolhar et al., 2005; Bolhar and Van Kranendonk, 2007 and Planavski et al., 2010). The formula for Eu anomalies is Eu/Eu*=Eu/(0.66Sm+0.33Tb) (Bau and Dulski, 1996). This equation does not use Gd as it is commonly anomalous.

Carbon dioxide and water contents were determined at Lakehead University using a CEC 240-XA Elemental Analyzer. Mineralogical analyses and elemental mapping were conducted using a JEOL 5900 scanning electron microscope and an energy dispersive spectrometer with a working distance of 10 mm.

Samples for chromium isotope analysis were digested with mixed HNO_3 and HF (3:1) on a hotplate. Fluorides were dissolved by repeated fluxing with *aqua regia*. Prior to column chemistry to purify Cr from matrix elements, sample aliquots containing ~1 µg Cr were spiked with a ^{50}Cr-^{54}Cr double spike ($^{50}Cr/^{52}Cr$=462.9170, $^{53}Cr/^{52}Cr$=0.5798, $^{54}Cr/^{52}Cr$=354.45, calibrated at the Department of Geology, University of Illinois at Urbana-Champaign) so that the spike/sample ratio (i.e., $^{54}Cr/^{52}Cr$) was about 0.5.

Cr separation followed the method outlined in Planavsky et al. (2014), which is based on Schoenberg et al. (2008). Briefly, Cr separation was achieved using an ion exchange resin AG1-X8 (100-200 mesh) to separate Cr (VI) anions from matrix elements after Cr oxidation. Residual Fe was separated from Cr in 6 N HCl by passing it through a microcolumn filled with 0.3 ml AG 50W-X8 (200-400 mesh) cation resin following previous methods (Trinquier et al., 2008). The yield was higher than 80% for all samples. Given the large amount of Cr processed a blank correction was not performed.

Chromium isotopic compositions were measured on a Neptune Plus MC-ICP-MS housed in the Yale Metal Geochemistry Center in the Department of Geology & Geophysics. Purified Cr samples dissolved in 0.7 N HNO_3 with concentrations of ~100 ppb were introduced to the plasma with a PFA µFlow nebulizer (~50 µl/min) coupled with an Apex IR (Elemental Scientific) without additional N_2 gas or without membrane desolvation. The isotopes ^{49}Ti, ^{51}V and ^{56}Fe were measured to monitor and correct for isotopic interferences from ^{50}Ti, ^{50}V and ^{54}Fe. The unprocessed NIST SRM 979 standard was

analyzed after every three samples to monitor potential drift, which was <0.1% for the session. The average of the NIST SRM 979 standards (n=44) was -0.0008, with a standard deviation of 0.035. Processed NIST SRM 979 aliquots were within 0.05% of the mean of the unprocessed standards (n=2). Chromium isotopic composition is expressed using the traditional delta notion: $\delta^{53}Cr = [(^{53/52}Cr)sample/(^{53/52}Cr)SRM979-1]x1000‰$.

4. FIELD DESCRIPTIONS

Five typical Gunflint outcrops were sampled for this study: three of the capping limestone and two of ankeritic carbonates (Figures 1 and 2). Outcrop area 1 lies near downtown Thunder Bay, whereas Area 2 is on the western outskirts and Area 3 lies on Highway 588 about 15 km west of the city (exact locations are given in Addison et al., 2010: Area 1 = Private Yard, Area 2 = GTP, Area 3 = Hwy 588). The two ankeritic outcrops are in the northeastern part of the city: Area 4 is on the Current River at Lyon Boulevard, whereas Area 4B is at a rock-cut on the TransCanada Highway 1 km west of Current River. Strata at these latter two locations are near the top of coarsening-upward cycles (Figure 2) and represent deposition in very shallow water.

At Area 1, the base of the sequence consists of silicified and pyritiferous ankerite overlain by horizontal, crinkly microbialite layers that locally develop into randomly spaced, hemispherical stromatolites, averaging 30 cm wide and 20 cm high (Figure 3A). Five centimeters of very coarse grainstone containing intraformational chlorite-bearing clasts and stromaclasts (Figure 3B) overlie the flat microbial layers and surround the

bases of the stromatolites. The coarse grainstone is overlain by about 3 cm of fine-grained grainstone with only chloritic clasts capped by 3 cm of very coarse grainstone. These layers are banked-up against the stromatolites and pass over them in places. Small channels are eroded between the stromatolites and filled by very coarse grainstone (Figure 3A). Pervasive blocky calcite cement is apparent in hand sample (Figure 3B and C). An erosive truncation surface cuts through the grainstones, removing the tops of some stromatolites. Overlying this surface is a pebble to boulder conglomerate produced by the Sudbury meteorite impact event (Addison et al., 2010) (Figure 3D), which has a matrix composed of fragments of devitrified vesicular glass (Figure 3E), chloritic sand, and sub-rounded to angular quartz grains with pervasive blocky calcite cement. The larger clasts are mostly composed of underlying limestone lithologies and black chert from the upper Gunflint Formation. This conglomeratic unit is only about 80 cm thick here due to truncation by recent erosion.

Area 2 is an abandoned railway cut through a bedrock knob composed primarily of clast-supported boulder conglomerate representing the base of the Sudbury impact layer (Figure 4A). The generally angular clasts are composed of chert, partially silicified ankerite grainstone, and limestone slabs up to 3.5 m in length (Figure 4B) as well as smaller pieces (Figure 4C). The slabs are lithologically identical to the limestone in Area 1. The matrix of the conglomerate is ankeritic sand with sub-millimeter to cobble-sized black chert clasts. The conglomerate is capped by 0-30 cm of devitrified, vesicular glass clasts, spherules and black chert clasts with blocky calcite cement (Figure 4D). Both sub-rounded and angular fine- to coarse-grained quartz grains are present among the

devitrified glass clasts. Rarely, the quartz grains contain poorly defined surfaces similar to planar deformation features produced by meteoric impacts. The devitrified, glass-rich layer also contains millimeter to cobble-sized, broken stromatolite clasts.

In Area 3, a basal, partially silicified, ankeritic grainstone is overlain by Limestone member grainstones and stromatolites similar to those in Area 1 (Figure 5A). Post-lithification these units were fractured, probably by earthquakes generated by the Sudbury impact event, with overlying sediment filling the fractures (Addison et al., 2010). The upper contact of the Limestone member is erosional and locally cuts through the tops of stromatolites. A bed of accretionary lapilli, 5-25 mm in diameter, lies on this erosional contact (Figure 5B). The matrix to the accretionary lapilli contains sub-millimeter to small-pebble-sized black chert clasts and devitrified glass spherule clusters within calcite cement. Planar deformation features in quartz grains within the accretionary lapilli, together with age determinations of zircons recovered from the lapilli layer show that this layer is a product of the Sudbury impact event (Addison et al., 2010).

The stratigraphic successions in Areas 4 and 5 are similar to each other. These large outcrop areas are dominated by 1 to 30 cm-thick layers of medium-grained ankeritic grainstone. The grainstones are parallel-laminated, hummocky cross-stratified and trough cross-stratified (Figure 6A). The upper surfaces of layers show evidence of very early silicification (upward rotation of silicified grainstone plugs from the top of a layer into the base of the above layer during dewatering). The silicification was probably induced by reaction with the overlying seawater (Fralick, 1988). Totally silicified hemispherical

stromatolites (individuals and groups) are present on some bedding horizons. Angular, eroded fragments of these silicified stromatolites have been incorporated into the carbonate grainstones (Figure 6B). The uppermost grainstone at site 4A is completely silicified and overlain by a lithified rubble zone produced during sub-aerial exposure prior to deposition of overlying large stromatolitic mounds (Figure 2).

5. PETROLOGY

5.1 Upper Limestone Member

The grainstones of the Limestone Member at the top of the Gunflint Formation are composed of very angular, shard-like to sub-rounded, chloritic sand grains in a cement of calcite and quartz (Figure 7). The chloritic grains are high in iron based on SEM-EDS and XRD analyses (Figure 8). They have a fairly consistent composition at all limestone sites with average atomic percentages of Fe = 11.9, Mg = 6.82 and V = 0.48 percent. Although these grains of chloritized mafic ash dominate the fine grainstones, stromatolite fragments are also common constituents in the coarse grainstones, and in places are the dominant grain type. Patches of fine-grained quartz replace portions of some carbonate and chlorite grains. Others show internal fracturing with the fractures filled with blocky calcite cement or quartz. Similar blocky calcite cement fills the intergranular spaces. The composition of the calcite cement is fairly consistent, with average atomic percentages of Ca = 97.6, Mg = 0.78, Fe = 0.74 and Mn = 0.90 (normalized to 100%). Coarse grainstone at the top of the Limestone member has a mosaic of quartz cement filling areas once occupied by calcite cement. This commonly occurs along crystal borders of the blocky

calcite cement, generally with a preferred vertical orientation. The stratigraphically lowest layer of coarse grainstone has a more pristine blocky cement with fewer areas of quartz cement (compare Figures 7A and 7B). In the overturned block at Area 2 (Figure 4B), the uppermost grainstone (stratigraphically lowest) directly lies on the base of the inverted stromatolites. This grainstone layer is comparable to the lowest coarse grainstone in Area 1, in that stromatolite fragments are common and blocky calcite crystals dominate the cement, with few quartz-filled dissolution channel-ways. The stromatolitic fragments forming the grains are much larger in this layer, commonly 1 to 4 mm. The underlying, stratigraphically higher, coarse grainstone in the inverted block has abundant quartz-filled dissolution channel-ways (Figure 7C) similar to the upper grainstone at Site 1 (Figure 7B). This indicates that quartz replacement of the blocky calcite cement was produced by fluids infiltrating from above before inversion of the large block. This infers that the quartz replacement occurred in the vadose zone during subaerial exposure prior to the Sudbury impact event.

The very fine-grained grainstones are well sorted with an average grain size of 0.1 mm. Grains are mostly black, oval to angular shards, and dominantly composed of iron-rich chlorite. The fine grainstones also contain abundant opaque minerals, the margins of which are stained with iron oxides. The blocky calcite cement in the fine grainstones is chemically similar throughout the area, and similar to that in the stromatolites and coarse grainstones, though it is not as abundant in the fine grainstones.

The stromatolites are composed of alternating thin layers of coarse, blocky calcite cement and laminations of opaque clastic material rich in high-iron chlorite (Figure 7D). The chlorite-rich grains may be opaque as a result of disseminated, fine-grained iron oxides. The chloritic laminations have Fe, Mg and V atomic percentages of 11.2, 7.64 and 0.44 percent, respectively, which are similar to values in the grainstones. Vanadium contents are fairly consistent between sites. The composition of the calcite cement is also consistent between sites, with average atomic percentages of: Ca = 97.5, Mg = 1.12, Fe = 0.80 and Mn = 0.55 (normalized to 100%). Grains of authigenic apatite are present, both in the cement, and in chloritic layers and clasts. The cement also contains rare small authigenic crystals of monazite.

5.2 Sudbury Impact Layer

In Area 1, the interstitial spaces between grains composing the devitrified granule and pebble matrix of the Sudbury impact boulder conglomerate are primarily filled with blocky calcite cement. The devitrified material is now mostly Mg-rich chlorite; a very different composition compared to the Fe-rich chloritic in the sand-sized clasts of the underlying grainstones. The chlorite in the impact layer conglomerates has a composition in atomic percentages of: Mg = 11.6%, Fe = 7.3% and V < 0.1%. Within the matrix of the conglomerate, granules and pebbles commonly show zoned devitrification. In areas where calcite cement is not well-developed, the granules and pebbles are separated by ankerite (Figure 3E). Petrographic examination reveals that this latter matrix has been neomorphically recrystallized. The impact conglomerate at Area 2 has a texturally and compositionally similar matrix. In Area 3 interstitial material in the conglomerates

consists of earlier calcite cement which, in places, was overgrown by compositionally zoned ankerite crystals. Euhedral zircons recovered from the matrix of the impact conglomerate at Area 3 gave a U-Pb age of 1856±2 Ma (Addison et al., 2010). Agate veining is common in some areas of the impact conglomerate. The veins do not extend into units overlying the conglomerate, and only rarely extend into underlying strata. The veins are associated with silica that partially fills open spaces in the form of miniature stalactites and even smaller stalagmites (Figure 9).

5.3 Ankeritic Grainstones

The ankeritic grainstones in Areas 4 and 5 are texturally quite different from the Limestone member and the Sudbury impact units. The grainstones are composed of euhedral ankerite crystals ranging in size from 0.1 to 0.5 mm. Larger, highly silicified stromatolitic fragments are also present in the grainstone of Area 4 (Figure 6B). Stromatolites are absent from Area 5 and therefore the grainstones at this site do not contain stromatolite fragments. In both areas, the carbonate spar appears neomorphic and is cut by numerous stylolites. The chemical composition of the ankerite is fairly consistent at both sites with average atomic percentages of: Ca = 51.4, Mg = 35.6, Fe = 11.8, Mn = 0.38 (normalized to 100%).

6. GEOCHEMISTRY

Whole-rock chemical analyses of samples of the lithologies described above are given in the data depository. Relative to the ankerite grainstone, the Limestone member on average contains about 100 times more V; 20 times more REEs, Y, P and Cr; and 3 to 12

times more U, Sr, Ba, Al, Ti, Cu, Pb and Zn (Figure 10). The concentrations of Al and Ti are elevated in the limestones due to significant amounts of chlorite. However, elements such as V, Cr, U, P, REEs, Y, Sr and Ba do not co-vary with Al and Ti in the grainstones and stromatolites (Figure 11), indicating that their concentrations are not controlled by the amount of detrital siliciclastic material in the samples. Partial dissolution of the carbonate phase by weak acid solutions also indicated that the REEs are significantly concentrated in the cement phases in the limestone and the ankerite in the ankerite grainstones. The ankeritic grainstones have about twice as much Fe, Mg and Mn as the calcitic grainstones. Within the Limestone member, the fine-grained grainstones and the matrix of the overlying impact-generated conglomerates are not as enriched in V and REEs as the coarse grainstones and stromatolites (Figure 10).

REE patterns for the lithologies discussed are shown in Figure 12. Samples from the limestone unit (Figures 12A, B, C) exhibit pronounced Ce depletion (Figure 13). They are enriched in Gd and the other middle REEs (Figures 12A, B, C) with minor additional Eu enrichment, except for one stromatolite sample (Figure 12A,B,C and 13). The two fine grainstone samples differ from this trend, as they are heavy REE enriched. The majority of the calcite grainstones, stromatolites and impact layer conglomerate matrixes also exhibit small amounts of La enrichment. Samples from the matrix of the impact boulder conglomerate display only slight La and Gd enrichment, slight Ce depletion, and generally show more Eu enrichment then the limestone samples (Figures 12A, B, C and 13). They have lower REE concentrations than the Limestone Member samples and only minor to no middle REE enrichment. By comparison, some ankeritic grainstones have

large La and, to a lesser extent, Ce enrichments, and all have significant positive Eu anomalies (Figure 12D). The ankeritic grainstone patterns are consistent with the findings of other authors for sediment precipitated from the Gunflint Sea (Danielson et al., 1992; Supplementary Information of Frie et al., 2009,).

Chromium isotope data for selected samples are shown in Figure 14. There was a large range of Cr isotope values in the selected samples, with δ^{53}Cr ranging from -0.1‰ to 1.38‰. The maximum values are, thus far, the heaviest δ^{53}Cr values reported for any Archean, Paleoproterozoic or Mesoproterozoic rock. With the exception of one sample, all of the ankerite grainstone samples have lower δ^{53}Cr values than the calcite stromatolites and coarse grainstones. However, five of the seven ankerite grainstones do have elevated δ^{53}Cr values compared to Frei et al.'s (2009) data for their Gunflint samples. The ankerite samples reported here are very likely from deposits formed in shallower water than Frei et al.'s (2009), the ramifications of which are discussed in a latter section. The calcitic, fine-grained grainstones have both low Cr/Ti ratios and δ^{53}Cr values, probably both related to the large amounts of mafic volcanic ash, now chlorite, in these samples.

A regional study was also conducted to examine the V content of strata across the Gunflint shelf. One hundred and sixty-two samples were collected from five drill-holes through the Gunflint and equivalent Biwabik Formation to the south. Vanadium concentrations in these holes show a striking pattern (Figure 15). A V-enriched zone occurs in the northern portion of the shelf about fifty meters above the base of the

formation and lies directly below a previously described regression surface marked by subaerial exposure in the north (Fralick and Barrett, 1995). Although the maximum V values in this interval are near the crustal average, an increase in the V/Ti ratio and very limited detrital input reflects some V enrichment in this zone. The exposure surface corresponds to the break between the Lower and Upper Members of the Gunflint Formation of Goodwin (1960). A second zone that is considerably richer in V lies in the uppermost portion of the Gunflint and Biwabik Formations. Vanadium concentration generally increases toward the top of the formation through this zone

In summary, Fe and Mn are enriched in the ankeritic grainstones, whereas other redox-sensitive elements, such as V, U and Cr, have much higher concentrations in the capping limestones. High concentrations of V also extend down from the limestones into the upper part of the underlying iron formation. Lower in the Gunflint Formation, V is also enriched below a paleo-exposure surface. REE patterns for some of the ankeritic grainstones have positive La anomalies and all have positive Eu anomalies, whereas the limestones have negative Ce anomalies and small positive Eu anomalies. The $\delta^{53}Cr$ values for the coarse-grained calcite grainstones and stromatolites are high, whereas the ankerite grainstones range from crustal values to high. The matrix of the impact layer conglomerates has geochemical characteristics between those two groups.

7. DISCUSSION

7.1 Depositional Setting of the Limestone Member and Impact Layer

Regression of the Gunflint Sea and subaerial exposure of the land during the interval between deposition of the Gunflint and Rove Formations has been proposed on the basis of both sedimentological and geochronological grounds (Addison et al., 2005, 2010; Johnson et al., 2006; Fralick, et al., 2012). Core from drill-holes in Ontario show a shoaling-upward succession tens of meters thick in the upper part of the Gunflint Formation, immediately below the Limestone member. The uppermost 3 m are bleached white with intense silicification (Poulton et al., 2004; Frei et al., 2009). This is the interval below the limestone unit that carries elevated V concentrations in the northern outcrop area. This V enrichment probably resulted from a regression with resulting subaerial exposure, by analogy with the lower V anomaly that occurs at a known regression surface separating the Lower and Upper members of the Gunflint Formation (Fralick and Barrett, 1995).

The clasts present in the grainstones of the Limestone member are lithologically different from the grains that make up strata in the underlying Gunflint Formation. In addition, stromatolites in the Limestone member consist mostly of alternating chlorite and calcite layers, whereas stromatolites in the underlying Gunflint are chert with varying iron and carbon content. In Area 1, where exposure of the underlying strata is limited, the limestone rests on a heavily silicified surface that is probably analogous to the silicified zone observed in drill-cores at the top of the Gunflint. This uppermost silicified zone is interpreted to have formed during subaerial exposure of the Gunflint prior to limestone deposition. The peneplaned subaerial topography (Fralick and Barrett, 1995) could have supported large shallow lakes, or simply a wet surface on which microbial mats grew and

mafic volcaniclastic material was episodically introduced and reworked forming the chlorite-rich material. Alternatively, reflooding of the area after silicification of the uppermost Gunflint could have resulted in deposition of the calcite grainstones and stromatolites in this marine water mass. However, the lack of Fe and Si forming chemical sediments in these deposits, their very different mineralogy compared to the underlying Gunflint and the evident freshwater diagenesis they underwent makes this latter scenario less likely.

The limestones overlying the silicified uppermost Gunflint are lithified by calcite and silica cements that formed prior to the 1850 Ma impact event. The silica fills open spaces in calcite along blocky calcite crystal boundaries that extend downwards into the rock. The quartz cement filling dissolution pathways along calcite crystal boundaries and also cross-cutting calcite crystals is much more common near the top of the Limestone Member. In overturned blocks of limestone found in the overlying impact conglomerate these silica-filled channel-ways are more common on the bottom surfaces of the blocks and extend up into them. This configuration indicates that the silica cements formed from downward moving fluids prior to inversion of the blocks, and thus represent a preexisting vadose setting. Given that the large clasts were lithified prior to being torn up and redeposited by an impact-related base-surge, the calcite cement in these rocks formed prior to 1850 Ma. The blocky nature of the calcite is typical of phreatic, meteoric cements (Land, 1970; Thorstenson et al., 1972; James and Choquette, 1990). The calcite cement is unlikely to have formed as a precipitate from the Gunflint Sea, because carbonate cements documented in the marine portion of the Gunflint are ankerite or siderite. Also in

support of a meteoric origin is the lack of fibrous, isopachous or inclusion-rich cements, all typical of marine cement. It is also unlikely marine water containing significant amounts of dissolved Fe^{+2} could precipitate a calcite cement (Sumner, 1997; Sumner and Grotzinger, 2000; Riding et al., 2014; Fralick and Riding, 2015).

The origin of the layer of chaotic debris overlying the Gunflint Formation in the northern outcrop area has been attributed to earthquake-induced fracturing of the upper bedrock surface, followed by transport of clasts by a high-velocity, base-surge cloud that expanded away from the Sudbury impact site (Addison et al., 2008; 2010; Fralick et al., 2012). This event, which occurred at 1850±1 Ma (Krogh et al., 1984), is the second-largest known impact in the history of the Earth (Spray et al., 2004; Earth Impact Database, 2004). The Sudbury impact produced an ejecta layer that is now found between the upper Gunflint and overlying Rove Formation and equivalent strata in Ontario, Minnesota, Wisconsin and Michigan (Addison et al., 2005; Pufahl et al., 2007; Jirsa, 2008; Cannon et al., 2010). The debris-rich conglomerate layer described here not only contains reworked pebbles to boulders of underlying lithologies, but also lapilli and accretionary lapilli, abundant devitrified glass and planar deformation features in quartz (Addison et al., 2008; 2010). These features have also been reported from geographically separate occurrences of the same debris-rich layer (Addison et al., 2005; Pufahl et al., 2007).

A U-Pb age determined on detrital zircons recovered from the matrix of the ejecta-bearing conglomeratic layer overlying the Gunflint Formation provides a lower age limit

for this unit of 1856±2 Ma (Addison et al., 2010). This supports the idea that the conglomeratic layer was formed by the 1850±1 Ma Sudbury impact event. Given that Penokean and Trans-Hudson volcanism occurred throughout the 1860 to 1832 Ma interval (Sims et al., 1989; Gordon et al., 1990), it is plausible that surface volcanic ash was locally present at the time of the impact and was caught-up in the base-surge cloud, thereby providing a source for the zircons now found in the matrix of the conglomeratic layer. If so, the volcanic ash was some 4-8 Ma older than the impact event .

The debris-rich Sudbury ejecta layer in the northern portion of the basin also commonly contains blocky calcite cement. Though it must have formed later, this cement is petrographically similar to that in the underlying limestone. In many areas agate veins also developed prior to deposition of overlying Rove strata and associated quartz stalactites and stalagmites (Figure 9) formed in the vadose zone by downward-percolating fluids.

7.2 Behavior of Redox-Sensitive Metals and REEs during Gunflint Deposition and Diagenesis

7.2.1 Vanadium and Uranium

The limestone unit that caps the Gunflint Formation contains intraformatonal stromatolite clasts and chlorite-rich grains with calcite cement (Figure 7). It is unlike other rocks in the Gunflint Formation or stratigraphic equivalents to the south. Hessler and Simonson (1989) found vitric grains, ash peloids and welded shards in similar chloritic strata near

Area 3 of the present study, and concluded that these constituents were derived from reworked mafic volcanic ash. . Further evidence for the presence of volcanic ash forming the chlorite-bearing clasts in the limestone are 1856 Ma zircons in the Sudbury impact debris (Addison et al., 2010). The only possible local source for these zircons is volcanic material. There are also numerous volcanic ash layers in the upper Gunflint and lower Rove Formations indicating ongoing volcanism.

The very high V contents (average of 1.5% V_2O_3) in the chlorites making-up the altered tuffaceous particles are highly unlikely to be primary. Preferential addition of V to the upper limestone is suggested by whole rock V/Al_2O_3 ratios that are consistently 10 to 100 times higher than those of the Gunflint ankerite grainstones (Figure 11). On the regional scale, V values are highest immediately below the paleo-erosional top of the Gunflint, generally decreasing to background values by 25-50 meters below this surface (Figure 15). This suggests that V enrichment occurred during subaerial exposure, presumably due to percolation of meteoric waters through the organic-rich carbonate sediment after it leached V from volcanic ash layers.

Similarities exist between the V-U concentrations in the Gunflint limestone and Mesozoic V-U deposits of the Colorado Plateau. Most of the V in the Colorado deposits occurs in chlorite (Northrop and Goldhaber, 1990), where it substitutes for Al in the octahedral sites (Breit and Wanty, 1991). In these deposits V and U were introduced into fluvial sandstones of the Morrison Formation by low-temperature groundwater prior to compaction of the sediment (Northrop and Goldhaber, 1990). The V content directly

correlates with the organic carbon content of the Mesozoic deposits. Precipitation of V was driven by reduction of the vanadate (plus V) or vanadyl (plus IV) ion to the plus 3 state; the V then may have precipitated as oxyhydroxides (Hostetller and Garrels, 1962; Northrop and Goldhaber, 1990; Wanty and Goldhaber, 1992). Vanadium is much more soluble in oxidizing water than in reducing water (Sugiyama, 1989; Shiller and Mao, 1999, 2000), and its solubility can be further increased if it forms complexes with sulfate (Wanty and Goldhaber, 1992). This leads to V dissolving and remaining in solution in oxygenated soil profiles (Marsh, 1991). If an oxidized solution containing V becomes reduced some V will precipitate (Wehrli and Stumm, 1989; Shiller and Mao, 2000). In the Colorado Plateau sandstones, organic matter and the hydrogen sulfide generated from it created reducing conditions that led to V precipitation. If oxidized solutions containing dissolved V diffuse into black shales and marls, which are rich in bitumen and organic matter, the V is precipitated onto organic compounds, such as tetrapyrrole (Lewan and Maynard, 1982), or forms vanadyl porphyrins (Premovic et al., 1986; Wanty and Goldhaber, 1992). During diagenesis of the Colorado Plateau sediments the V, which would have been present either as oxyhydroxides or organic complexes, was incorporated into smectite as it altered to chlorite (Northrop and Goldhaber, 1990). By analog with the Colorado Plateau, we therefore interpret the elevated V in the limestone as being originally derived from volcanic ash by oxidized groundwater, and then fixed by contact with organic derived reductants in the limestone.

As noted earlier, the stromatolites and coarse grainstones of the Gunflint Limestone member contain elevated amounts of V (Figure 10). These two lithofacies also contain a

large amount of microbially generated material (fragments of the stromatolites form a major constituent of the coarse grainstones). Both lithofacies would have had high porosity and permeability before cementation. Fine grainstones, by contrast, have lower V contents, contain less stromatolitic debris, more tuffaceous material and more rounded grains. The lower V contents of the fine grainstones may be due to lower amounts of primary organic material combined with lower porosity and permeability. The conglomerates have intermediate V contents (Figure 10), as they are mixtures of V-enriched limestone debris and low-V material eroded from underlying units in the Gunflint Formation.

Uranium behaves during changing oxidation states in a manner similar to V during redox transformations, as discussed in Brown (2003). In the Gunflint Formation, the capping limestone contains considerably more U than underlying ankeritic grainstones (Figure 10B). This strongly suggests that the U, like V, was precipitated from fluids that were originally oxidized, but which became reduced as they diffused through the limestone sediment.

7.2.2 Chromium

The Gunflint limestones and matrix of the impact conglomerate have 20 times more Cr, on average, than the underlying ankeritic grainstones (Figure 10A). Chromium-aluminum ratios (Figure 11A) indicate that the concentration of Cr is not related to the amount of mafic tuffaceous material present. In fact, Cr co-varies with V, suggesting that it was oxidized to the VI state in the subaerial realm, and behaved in a similar manner to V in

the groundwater system. In rocks of the continental crust, chromium is present in the +3 state and is relatively immobile under an anoxic atmosphere with fluids at near-neutral pH. If enough oxygen is present in the atmosphere to oxidize manganese, the resulting manganese oxide can oxidize Cr to the +6 state (Eary and Rai, 1987; Oze et al., 2007). The Cr then becomes mobile and can be transported in oxidized groundwater. If that groundwater enters a reducing environment, the dissolved Cr can revert back to the +3 state and precipitate. Such a sequence of events is invoked here to explain the Cr enrichment in the organic-rich Limestone member.

Chromium isotopes provide additional insights into the alteration process and the mechanisms driving the observed Cr enrichments. The Cr isotope system is unique in that the isotopic composition of Cr in low-temperature rocks is controlled almost exclusively in most cases by redox transformations (Johnson and Bullen, 2004). There is a narrow range of Cr isotope values (reported as δ^{53}Cr) in igneous systems, with an average value of -0.12‰ (±0.1 2SD) (Schoenberg et al., 2008). Because Cr is present in igneous rocks exclusively as Cr (III), the initial Cr reservoir for terrestrial weathering will be stable under reducing conditions. Both theoretical and experimental studies indicate that Cr undergoes limited fractionation during non-redox-dependent transformations (Ellis et al., 2004; Johnson and Bullen, 2004b; Schauble et al., 2004), as indicated by the common occurrence of sedimentary rocks with authigenic Cr enrichments that have crustal or near-crustal Cr isotope compositions (e.g., Schoenberg et al., 2008; Frei et al., 2009; Planavsky et al., 2014).

In marked contrast to non-redox processes, oxidation and reduction of Cr induce large isotope fractionations. At equilibrium, the $Cr(VI)O_4^{2-}$ anion is enriched by over 6‰ relative to the parent Cr(III) reservoir (Schauble et al., 2004). However, the oxidation fractionation is smaller in experimental systems explored thus far (Zink et al., 2010). Kinetic fractionations between Cr (VI) and Cr(III) during reduction are typical in natural systems and range between 3 and 5.5‰ (Ellis et al., 2002; Ellis and Johnson, 2004; Johnson and Bullen, 2004; Schauble et al., 2004; Zink et al., 2010). Thus, the redox cycling of Cr leads to large Cr isotope fractionations. Modern groundwaters are consistently isotopically enriched, which is typically attributed to partial reduction of a soluble Cr(VI) reservoir (Johnson and Bullen, 2004).

The extremely positive $\delta^{53}Cr$ values observed in the meteorically altered samples must be tied to capture of a Cr(VI) reservoir. Similar to modern groundwaters, the positive values can be linked to partial reduction during groundwater flow. The markedly positive Cr isotope values provide compelling evidence that the enrichments are the result of low temperature groundwater alteration, rather than high temperature mineralization. The presence of very isotopically enriched Cr in the strongly meteorically altered upper portion of the Gunflint is also relevant to previous Cr isotope work in the formation. Frei et al. (2009) observed a shift in $\delta^{53}Cr$ values in the upper portion of the Gunflint Formation, with the presence of small positive $\delta^{53}Cr$ values in the upper 25m of the Formation. The Cr enrichment trend matches the V enrichments and is likely due to infiltration of the meteoric waters through volcanic ash during subaerial exposure following regression of the Gunflint Sea.

The presence of a thick zone of alteration (~25 meters for Cr and V) implies deep penetration of initially oxic groundwater. The large trace mineral enrichments are tied to local reduction of redox-sensitive metals, indicating the flow of oxic groundwaters through Gunflint sedimentary rocks, which contain large amounts of reductants (e.g. ferrous iron). Given that the alteration seems to be spatially pervasive (Fig. 15) it is unlikely that the oxic groundwaters penetrated to deeper levels only in limited areas of unusually high porosity characterized by rapid water flow with limited host rock interaction. Therefore, all the evidence from redox-sensitive metal enrichments and isotopes is consistent with the presence of significant oxygen in the atmosphere at the end of Gunflint deposition and prior to meteorite impact at 1850 Ma.

Chromium isotopes have been used as a quantitative paleoredox proxy (e.g., Planavsky et al, 2014). Translating Cr isotope records into an estimate of pO_2 levels relies on coupling of several reactions – Cr(III) going into solution, Mn being oxidized, and Cr being oxidized by Mn oxides – that have "known" rate laws (Planavsky et al, 2014). In this approach – since it is building from a kinetic framework – one must assume reaction durations. Sedimentary systems are likely to record geochemical signatures of terrestrial processes that reflect average water residence times and soil development times of the source catchment. Paleosols and facies affected by groundwater, in contrast, will record the integrated product of a possibly protracted alteration process. In this light, care must be taken when comparing signatures of terrestrial processes in sedimentary rocks and terrestrial archives. Rybacki et al. (2016) recently outlined how variable soil

development times affect soil redox properties at various atmospheric oxygen levels and highlighted how soil development times affect pO_2 reconstructions. In this light, it is difficult to translate our observations into a quantitative pO_2 estimate. However, future reactivation transport modeling, ideally with better estimates of exposure times in the Gunflint system, may be able to provide a quantitative estimate of atmospheric oxygen partial pressures based on signatures of oxic groundwaters altering the Gunflint system.

The large range of $\delta^{53}Cr$ values for the shallow-water ankerite grainstones may be tied to the mixing of two water masses with differing Cr isotopic ratios: the offshore ocean with slightly negative values (Frei et al., 2009, Figure 3) and continentally derived water with large positive values (data from this study). The ankerite grainstones analyzed were from very shallow-water settings with nearshore current reworking of the sands immediately prior to episodes of maximum regression. This contrasts with the farther offshore locations where Frei et al.'s (2009) samples were deposited. Changing flux rates into the very shallow settings where our ankerite grainstone samples accumulated would account for their variation in $\delta^{53}Cr$. Wetter periods with increased runoff would raise the ratio, while drier periods or increased importance of offshore-directed winds and resultant upwelling or storm surges (Pufahl and Fralick, 2004) would lower the ratio. Localized variability in $\delta^{53}Cr$ values has been noted in the modern ocean with increased values of up to +1.51‰ (Bonnand et al., 2013) driven by continental runoff into the nearshore marine environment (Scheiderich et al, 2015). This is comparable to our highest value of +1.17‰ for near-shore ankerite grainstone. However, all of the Cr isotopic variability could be the result of later Paleoproterozoic groundwater alteration.

7.2.3 Phosphorus

Phosphorous is also strongly enriched in the calcite grainstones compared with the Gunflint ankerite grainstones (Figures 10C, 11B). Scanning electron microscope analysis indicates that P occurs as apatite and monazite intergrown with the calcite cement. This suggests that the P precipitated from the same fluid that formed the cement and because the cement in the limestone is pre-Sudbury impact the REE-bearing minerals probably are too. The low P values for the underlying ankerite grainstones are comparable to the low amounts of P reported by Bjerrum and Canfield (2004) for samples from the correlative Biwabik iron formation and other Archean and Paleoproterozoic iron formations. These authors related the low amounts of phosphate in the iron formations to much lower levels of P in the Archean and Paleoproterozoic paleo-oceans, although there has been extensive debate on this topic (e.g., Jones et al., 2015 and references therein). The large amounts of phosphate associated with the blocky cements of the Gunflint limestone indicate that these cements were not precipitated from seawater.

7.2.4 Rare Earth Elements

The calcite cements in the Limestone Member have consistent REE patterns that are strikingly different to those of the Gunflint ankerites lower in the succession (Figure 12). Relative to the Gunflint limestone samples, oxidized groundwater from modern upland areas (Gruau et al., 2004) has a very similar REE pattern, including significant Ce depletion and enrichment in the middle REEs (Figure 16). By contrast, groundwater from a nearby wetland, which has a lower redox potential then the upland groundwaters,lacked

a Ce anomaly, but did exhibit the humped, middle REE enriched pattern (Gruau et al., 2004) (Figure 16). These authors concluded that Ce in the upland groundwater was oxidized to Ce(IV) and removed either by direct precipitation or by oxidative scavenging on the surfaces of Fe and Mn oxyhydroxides forming in the soil. Soils from various modern climatic zones typically exhibit Ce enrichment, which is commonly ascribed to either: 1) oxidation of dissolved Ce(III) and formation of cerianite (CeO_2), commonly as globules adhering to minerals in Mn oxide-rich areas; or 2) oxidation and scavenging of dissolved Ce(III) by Mn oxyhydroxides (Rankin and Childs, 1976; Lei et al., 1986; Marsh, 1991; Koppi et al., 1996; Braun et al, 1998; Bau, 1999; Ohta and Kawabe, 2001; Ji et al., 2004). Such precipitation processes lead to negative Ce anomalies in both surface water (Sholkovitz, 1995) and groundwater (Smedley, 1991; Braun et al., 1998; Dia et al., 2000; Compton et al., 2003). Because of the sensitivity of dissolved Ce to redox conditions, combined with the stability of REE signatures in calcite (Zhong and Mucci, 1995; Cherniak, 1998; Webb et al., 2009), there has been widespread use of Ce anomalies as a proxy for Eh (Wright et al., 1987; Liu et al., 1988; Murray et al., 1990; Holser, 1997; Bau et al., 1998; Yang et al., 1999; Kamber et al., 2004). The Ce-depleted, middle REE enriched REE patterns of the Gunflint capping limestone are similar to those of modern groundwater that has traveled through an oxidized area where Mn or Fe oxyhydroxides have formed.

The REE patterns for the ankeritic grainstones are typical of oceanic precipitates from the Paleoproterozoic and the Archean (for comparative patterns see: Barrett et al., 1988; Fralick et al., 1989; Murray et al., 1990; Danielson et al., 1992; Bau and Moller, 1993;

Bau and Dulski, 1996; Bellanca et al., 1997; Yang et al., 1999; and, Webb and Kamber, 2000). In general, the ankeritic grainstones exhibit some features typical of modern seawater REE patterns, but they lack negative Ce anomalies and heavy REE enrichment. The REE patterns of the Gunflint ankeritic grainstones do, however, have the positive Eu anomaly that is commonly found in modern vent fluids and some metalliferous sediments (Barrett et al., 1988; Michard et al., 1993; Cocherie et al., 1994; German et al., 1999). In general, Archean and early Paleoproterozoic iron formations show similarities to modern vent fluids, which have been used to suggest that the chemistry of the early oceans was strongly influenced by sub-seafloor hydrothermal circulation (Jacobsen and Pimentel-Klose, 1988; Derry and Jacobsen, 1990; Danielson et al., 1992; Alibert and McCulloch, 1993; Bau and Dulski, 1996). In particular, a positive Eu anomaly in hydrothermal vent fluids provides evidence that some of the REEs were leached from rock of the ocean crust by fluids in excess of 175° to 250° C (Sverjensky, 1984; Danielson et al, 1992). Most of the Gunflint limestone samples, by contrast, have small positive Eu anomalies (Figures 12 and 13). This provides additional evidence that the cements in the limestones did not precipitate from marine pore waters, but rather terrestrial waters. Dissolution of Gunflint ankeritic carbonates on land with significant oxygen present would result in the fluid phase having a negative Ce anomaly, but also a positive Eu anomaly, which it would inherit from the ankerite. Thus, the presence of a small positive Eu anomaly in the Gunflint limestones indicates that the majority of REEs in the fluids that formed the cements in these rocks were derived from leaching of non-Gunflint rock types that did not have a Eu anomaly.

7.2.5 Implications of Geochemical Data

Although the Gunflint ankeritic grainstones that were sampled were deposited in shallow enough depths to be affected by storm reworking, and likely fair-weather waves (Fralick, 1988), their REE patterns are similar to those of sediment precipitated in deeper areas of the shelf (see data in: Danielson et al., 1992; Planavsky et al., 2009; Frei et al., 2009). These patterns indicate that the Gunflint iron-rich sediments were primarily derived from fluids that were deficient in oxygen. This contrasts with iron formation models that invoke the presence of oxygen-bearing waters across much of the shelf. We suggest instead that very near-shore waters contained some oxygen generated from photosynthesis, runoff of continental surface and groundwater, and diffusion from the atmosphere, and that these oxygen-bearing waters mixed with Fe^{+2}-bearing waters on the middle and outer shelf during storm events leading to precipitation of Fe hydroxides (e.g., Pufahl and Fralick, 2004).

The capping limestone of the Gunflint Formation provides information on the sub-aerial environment. Vanadium and uranium were precipitated from groundwater where it encountered organic/hydrocarbon-bearing, reducing stromatolitic sediments, and became sequestered in meteoric calcite cement. REE patterns of cements in the stromatolitic sediments also reflect groundwater chemistry. These chemical data point towards significant levels of atmospheric oxygen during at least the very latest Gunflint times, although highly reducing conditions prevailed in the deep oceans and across much of the shelf prior to this, and possibly after the Sudbury impact event, because ankerite grainstones locally overlie the impact layer.

Paleosol studies also point to oxidizing conditions in Late Paleoproterozoic regolith. Driese at al. (1995) report evidence for the oxidation of Mn and Fe in paleosols of the 1.8 Ga Lochness Formation in northern Australia, whereas Pan and Stauffer (2000) found a positive Ce anomaly, as well as cerianite, in a 1.85 Ga paleosol at Flin Flon, Manitoba, Canada. A simple Fe and O_2 model has been used to suggest that atmospheric oxygen concentrations during Gunflint deposition were no greater than about 0.1 percent of present levels (e.g., Canfield, 2005). Twice this level of oxygen has been inferred from the presence of positive Ce anomalies in the Flin Flon paleosol (Pan and Stuaffer, 2000), which is consistent with our observations of Ce oxidation in terrestrial environments and deep penetration of oxic groundwater. The latter results were taken to indicate that atmospheric pO_2 had a minimum value of $10^{-1.5}$ to 10^{-2} PAL. This apparent contradiction may be the result of intense hydrothermal activity and upwelling of reductants onto shelves. There was a large pulse of igneous activity at about this time – the ca. 1.88 Ga ultramafic large igneous province (LIP) (Heaman et al., 1986, 2009; Hulbert et al., 2005). The LIP has been proposed as having been linked to a mantle plume breakout event (Hamilton et al., 2009; for a different view see Heaman et al., 2009). There are iron formations similar in age to the Gunflint (Ricketts et al., 1982; Fralick et al, 2002; Schulz and Cannon, 2007) and extensive coeval submarine, basaltic volcanism (Findlay et al., 1995; Fralick et al, 2002; Schneider et al., 2002) for thousands of kilometers along the edge of Superior craton and in western Australia (Rasmussen et al., 2012). It has been proposed that this peak in global mafic-ultramafic magmatism (French et al., 2008, Heaman et al., 2009, Ernst and Buchan, 2010, Meert et al., 2011) created a high flux rate

of reductants to the world ocean, overwhelming the oxygen flux and producing widespread ferruginous conditions in the marine environment (Rasmussen et al., 2012). The increased Fe flux would have also led to nutrient stress (via Fe oxide P scavenging), stabilizing the ocean-atmosphere system at low levels while there were high ferrous Fe fluxes to the oceans. Thus, available evidence suggests that there were exceptionally high rates of world-wide, submarine hydrothermal activity resulting in relatively anoxic oceans. However, significant levels of oxygen were maintained in the terrestrial environment.

In contrast to Gunflint marine records, Gunflint terrestrial archives indicate a well-oxygenated system. The main stage of iron formation meteoric alteration occurred after the main pulse of iron formation deposition and after LIP emplacement. Therefore, the possibility may exist that we are capturing a signal for a highly dynamic ocean-atmosphere system; one that was capable of significant changes to its oxygen concentration over only a few tens of millions of years. Complicating this situation is the presence of carbonate iron formation overlying the Sudbury ejecta layer in a number of drill-cores and outcrops (Figure 2). The existence of iron formation above the ejecta layer negates the argument of Slack and Cannon (2009) that the impact caused ocean turnover ending iron formation deposition and indicates that at least a somewhat ferruginous ocean continued in its shallow areas after meteoric alteration of the underlying sediments.

The paleosol studies of Driese et al. (1995) and Pan and Stauffer (2000) provide further evidence for significant amounts of oxygen in the atmosphere at least during intervals at

approximately 1.85 Ga. Other work, such as the documented loss of Mn from a 1.1 Ga paleosol in Michigan (Zimben and Holland, 1988), suggests lower oxygen levels in the Mesoproterozoic. Such a condition is also consistent with limited Cr isotopic fractionation in a suite of Mesoproterozoic ironstones, in strong contrast to Phanerozoic ironstones, which suggests limited coupled terrestrial Mn-Cr cycling and low Mesoproterozoic atmospheric oxygen levels (Planavsky et al., 2014). Therefore, the observed signal for high atmospheric oxygen concentrations at ca. 1860 Ma, coupled with other constraints on Proterozoic atmospheric oxygen levels, appears to provide additional support for the idea of large swings in pO_2 levels, in contrast with the traditional view (Holland, et al., 2005) of a unidirectional rise of surface oxygen levels on Earth. As noted above, modeling the observed oxic alteration profiles may provide a quantitative rather than qualitative estimate of pO_2 variations.

8. CONCLUSIONS

U-Pb age determinations on zircons from volcanic ash (Fralick et al., 2004; Addison et al., 2005) confirm that two hiatuses exist at the top of the Gunflint Formation, which was deposited at about 1878 Ma. One hiatus, at the top of the Gunflint iron formation succession, lasts from about 1878 Ma until sometime before 1850 Ma and is recorded by silicification of the top 5 m of the iron formation. The Limestone member was deposited sometime between 1878 and formation of the Sudbury impact layer at 1850 Ma. It has a subaerial exposure surface at its top, during which time calcite and quartz cements formed in the sediment. The other hiatus lasted from 1850 Ma until about 1832 Ma,

exposed the Sudbury impact layer to subaerial processes and is recorded by meteoric phreatic calcite cements and vadose quartz cements in the impact layer. Minor re-flooding events may have occurred during this interval, explaining the deposition of 1 to 6 meters of ankeritic grainstone overlying the Sudbury impact layer. The presence of similar ankeritic grainstones both below and above the impact layer throws into question the argument of Slack and Cannon (2009) for an extraterrestrial demise of iron precipitation caused by the Sudbury impact event.

The wave-reworked ankerite sands deposited in near-shore areas of the Gunflint shelf have REE patterns similar to those of chemical precipitates deposited in off-shore areas (for comparison see: Danielson et al., 1992; Planavsky, 2009; Frei et al., 2009). The precipitation of iron carbonates in the near-shore part of a shelf that was over 150 kilometers wide requires transport of dissolved Fe^{+2} from deep ocean vent sources across this expanse. This necessitates that the shelf, or at least the part below fair-weather wave penetration, was anoxic. A surface layer with phytoplankton may have existed, but if so, it did not supply enough oxygen to interfere with the transport of dissolved iron across the wide shelf. Whether the shelf was somewhat oxygenated or relatively anoxic was controlled by rate of Fe^{+2} resupply from the ocean reservoir versus oxygenation of the surface layer and offshore physical mixing with oxygenated very near-shore water during storm events. The abundance of grainstones in the mid- and inner-shelf areas attests to the importance of storm events (Fralick, 1988; Pufahl and Fralick 2004). Thus, to maintain the predominantly anoxic conditions, Fe^{+2} resupply from the ocean had to outpace: 1) photosynthetic production of oxygen, 2) delivery of oxygenated groundwater

and surface water from the continent, and 3) diffusion and mixing of oxygen into the surface layer from the atmosphere.

Sediments composing the Limestone member in the uppermost few meters of the Gunflint Formation below the impact layer consist of stromatolites and grainstones. Both of these contain an important component of mafic volcanic ash and have blocky calcite cements. The stromatolites and grainstones were deposited in a very shallow-water, probably lacustrine environment or an area where the water table lay either at or very close to the surface. In this setting, early blocky calcite cement formed in the meteoric phreatic zone. The early calcite cements also enclose authigenic apatite and lesser monazite crystals. Later, in the vadose zone, silica cement was deposited along mainly sub-vertical boundaries between calcite crystals.

Subaerial exposure prior to the Sudbury impact event led to the capping Limestone member having a very different geochemistry relative to the underlying ankeritic grainstones in the Gunflint Formation proper. Highly elevated contents of V, U and Cr in the Limestone member strongly suggest that precipitation occurred where oxidized groundwater entered a reducing zone in the sediment column. The reducing zones were probably formed by the decay of organisms or hydrocarbons formed from their decay. REE patterns for the Limestone Member are similar to those of modern-day oxidized groundwater. The chemical results imply that meteoric water, during deposition of the Limestone member was oxygenated to the point where vanadium in the +IV or +V state,

Cr in the +VI state and U in the +VI state were maintained in solution, whereas Ce was oxidized to the +IV state and removed from solution.

Following deposition of the Limestone Member and lithification in a sub-aerial environment, the blast cloud from the Sudbury impact event reworked the earthquake-shattered, lithified strata of the upper Gunflint Formation (ie., the ankeritic grainstones and originally overlying limestones). Blocky calcite cement and siliceous cement were precipitated in the matrix of the impact debris, locally forming small quartz stalactites and stalagmites in vadose open spaces. Due to the mechanical mixing of ankeritic and limestone material the geochemistry of the impact debris is intermediate between these two lithologies.

Evidence from redox-sensitive metals points to oxidizing conditions on land during Gunflint times, even as reducing conditions existed in the oceans. This conclusion is consistent with available evidence from similarly aged paleosols. Therefore, during deposition of the Gunflint Formation there appears to have been an imbalance between redox states of the ocean and atmosphere, or variable atmospheric oxygen levels. This imbalance in the Animikie Basin could have been caused by a high delivery of reductants to the oceans from hydrothermal systems, causing the balance point between reductant flux and oxygen flux to be located close to shore. This condition highlights the importance of deciphering the geochemistry of Precambrian marine systems in terms of flux rates rather than absolute processes. These results also emphasize the importance of understanding spatial versus temporal geochemical variability in depositional

environments. Past geochemical models for Precambrian oceans have commonly only considered vertical chemical zonation. However, in shelf, platform and epeiric sea settings, where storm waves can cause mixing of the water column to substantial depths, geochemical gradients are more likely to develop laterally away from the shoreline, as recent work is beginning to acknowledge (Pufahl and Fralick, 2004; Poulton et al, 2010, Fralick and Riding, 2015).

ACKNOWLEDGEMENTS

This work was supported by Canadian NSERC Discovery Grants and a University Research Chair to PWF. We are indebted to Sam Spivak for drafting the figures.

REFERENCES

Addison, W.D., Brumpton, G.R., Vallini, D.A., McNaughton, N.J., Davis, D.W., Kissin, S.A., Fralick, P.W. and, Hammond, A.L., 2005, Discovery of distal ejecta from the 1850 Ma Sudbury impact event: Geology, v. 33, p. 193-196.

Addison, W.D., Brumpton, G.R., Fralick, P.W., and Kissin, S.A., 2008, The complex Gunflint-Rove Formations boundary at Thunder Bay, Ontario: two disconformities and a base surge debrisite: Institute on Lake Superior Geology, v. 55, p. 1-2.

Addison, W.D., Brumpton, G.R., Davis, D.W., Fralick, P.W., and Kissin, S.A., 2010, Debrisites from the Sudbury impact event in Ontario, north of Lake Superior, and a new age constraint: are they base surge deposits or tsunami deposits?, *in* eds.

Reimold, W.U., and Gibson, R.L., eds., Large Meteorite Impacts and Planetary Evolution IV: Geological Society of America Special Paper 465, p. 245-268.

Alibert, C., and McCulloch, M.T., 1993, Rare earth element and neodymium isotopic composition of the banded iron formations and associated shales from Hamersley, western Australia: Geochimica et Cosmochimica Acta, v. 57, p. 187-204.

Barovich, K.M., Patchett, P.J., Peterman, Z.E., and Sims, P.K., 1989. Nd isotopes and the origin of the 1.9-1.7 Ga Penokean continental crust of the Lake Superior region, Geological Society of America Bulletin, v. 101, p. 333-338.

Barrett, T.J., Fralick, P.W., and Jarvis, I., 1988, Rare-earth-element geochemistry of some Archean iron formations north of Lake Superior, Ontario: Canadian Journal of Earth Science, v. 25, p. 570-580.

Bau, M., 1999, Scavenging of dissolved yttrium and rare earths by precipitating iron oxyhydroxides: experimental evidence for Ce oxidation, Y-Ho fractionation, and lanthanide tetrad effect: Geochimica et Cosmochimica Acta, v. 63, p. 67-77.

Bau, M., and Dulski, P., 1996, Distribution of yttrium and rare-earth elements in the Penge and Kuruman iron-formations, Transvaal Supergroup, South Africa: Precambrian Research, v. 79, p. 37-55.

Bau, M., and Moller, P, 1993, Rare earth element systematics of the chemically precipitated component in Early Precambrian iron formations and the evolution of the terrestrial atmosphere-hydrosphere-lithosphere system: Geochimica et Cosmochimica Acta, v. 57, p. 2239-2249.

Bau, M., Beukes, N.J., and Romer, R.L., 1998, Increase of oxygen in the Earth's atmosphere and hydrosphere between –2.5 and –2.4 GA B.P: Mineralogical Magazine, v. 62A, p. 127-128.

Bekker, A., Holland, H.D., Wang, P.L., Rumble, D., Stein, H.J., Coetzee, L.L., and Beukes, N.J., 2004, Dating the rise of atmospheric oxygen: Nature, v. 427, p. 117-120.

Bellanca, A., et al., 1997, Rare earth elements in limestone/marlstone couplets from the Albian-Cenomanian Cismon section (Venetian region, northern Italy): assessing REE sensitivity to environmental changes: Chemical Geology, v. 141, p. 141-152.

Bjerrum, C.J, and Canfield, D.E., 2002, Ocean productivity before about 1.9 Gyr ago limited by phosphorus adsorption onto iron oxides: Nature, v. 417, p. 159-162.

Bolhar, R, and Van Kranendonk, M.J., 2007. A non-marine depositional setting for the northern Fortescue Group, Pilbara Craton, inferred from trace element geochemistry of stromatolitic carbonates. Precambrian Research, v. 155, p. 229-250.

Bohlar, R., Van Kranendonk, M.J., and Kamber, B.S., 2005. A trace element study of siderite-jasper banded iron formation in the 3.45 Ga Warrawoona Group, Pilbara Craton – Formation from hydrothermal fluids and shallow seawater. Precambrian Research, v. 137, p. 93-114.

Bonnand, P., James, R.H., Parkinson, I.J., Connelly, D.P., and Fairchild, I.J., 2013. The chromium isotopic composition of seawater and marine carbonates. Earth and Planetary Science Letters, v. 382, p. 10-20.

Braun, J.-J., Viers, J., Dupre, B., Polve, M., Ndam, J., and Muller, J.-P., 1998, Solid/liquid REE fractionation in the lateritic system of Goyoum, East Cameroon: the

implications for the present dynamics of the soil covers of the humid tropical regions: Geochimica et Cosmochimica Acta, v. 62, p. 273-299.

Breit, G.N., and Wanty, R.B., 1991, Vanadium accumulation in carbonaceous rocks: a review of geochemical controls during deposition and diagenesis: Chemical Geology, v. 91, p. 83-97.

Burnham, O.M., and Schweyer, J., 2004, Trace element analysis of geochemical samples by inductively coupled plasma mass spectrometry at Geoscience Laboratories: revised capabilities due to improvements to instrumentation: Ontario Geological Survey Open File Report 6145, p. 54.1-54.5.

Burnham, O.M., Hechler, J.H., Semenyna, L., and Schweyer, J., 2004, Minerological controls on the determination of trace elements following mixed acid digestion: Ontario Geological Survey Open File Report 6100, p. 36.1-36.12.

Canfield, D.E., 2005, The early history of atmospheric oxygen; homage to Robert M. Garrels: Annual Review of Earth and Planetary Sciences, v. 33, p. 1-36.

Cannon, W.F., Schulz, K.J., Horton, J.W., and Kring, D.A., 2010, The Sudbury impact layer in the Paleoproterozoic iron ranges of northern Michigan, USA: Geological Society of America Bulletin, v. 122, p. 50-75.

Cherniak, D.L., 1998, REE diffusion in calcite: Earth and Planetary Science Letters, v. 160, p. 273-287.

Church, S.E., 1981, Multielement analysis of fifty-four geochemical reference samples using inductively coupled plasma-atomic emission spectrometry: Geostandards Newsletter, v. 2, p. 133-160.

Cloud, P., 1972, A working model of the primitive Earth: American Journal of Science, v. 272, p. 537-548.

Cloud, P., 1973, Paleoecologecal significance of the banded iron-formation: Economic Geology, v. 68, p. 1135-1143.

Cocherie, A., Calvez, J.Y., and Oudin-Dunlop, E., 1994, Hydrothermal activity as recorded by Red Sea sediments: Sr-Nd isotopes and REE signatures: Marine Geology, v. 118, p. 291-302.

Compton, J.S., White, R.A., and Smith, M., 2003, Rare earth element behavior in soils and salt pan sediments of a semi-arid granitic terrain in Western Cape, South Africa: Chemical Geology, v. 201, p. 239-255.

Danielson, A., Moller, P., and Dulski, P., 1992, The europium anomalies in banded iron formations and the thermal history of the ocean crust: Chemical Geology, v. 97, p. 89-100.

Davranche, M., Pourret, O., Gruau, G., Dia, A., and Le Coz-Bouhnik, M., 20005, Adsorption of REE(III)-humate complexes onto MnO_2; experimental evidence for cerium anomaly and lanthanide tetrad effect suppression: Geochimica et Cosmochimica Acta, v. 69, p. 4825-4835.

Derry, L.A., and Jacobsen, S.B., 1990, The chemical evolution of Precambrian seawater: Evidence from REE's in banded iron formation: Geochimica et Cosmochimica Acta, v.54, p. 2965-2977.

Dia, A., Gruau, G., Olivie-Lauquet, G., Riou, C., Molenat, J., and Curmi, P., 2000, The distribution of rare-earths in groundwater: assessing the role of source-rock

composition, redox changes and colloidal particles: Geochimica et Cosmochimica Acta, v. 64, p. 4131-4151.

Earth Impact Database, 2004, Earth Impact Database: www.unb.ca/passe/ImpactDatabase (accessed October 2004).

Driese, S.G., Simpson, E.L., and Eriksson, K.A., 1995, Redoximorphic paleosols in alluvial and lacustrine deposits, 1.8 Ga Lochness Formation, Mount Isa, Australia: pedogenic processes and implications for paleoclimate: Journal of Sedimentary Research, v. A65, p. 675-689.

Eary, L.E., and Rai, D., 1987, Kinetics of chromium (III) oxidation to chromium (VI) by reaction with manganese dioxide: Environmental Science and Technology, v. 21, p. 1187-1193.

Ellis, A.S., Bullen, T.D. and Johnson, T.M., 2002, Chromium isotopes and the fate of hexavalent chromium in the environment: Science, v. 295, p. 2060-2062.

Ellis, A.S., Johnson, T.M., and Bullen, T.D., 2004, Using chromium stable isotope ratios to quantify Cr (VI) reduction: Lack of sorption effects: Environmental Science and Technology, v. 38, p. 3604-3607.

Ernst, R.E., and Buchan, K.L., 2010, Large igneous provences (LIPs) and carbonatites: Mineralogy and Petrology, v. 98, p. 55-77.

Findlay, J.M., Parrish, R.R., Birkett, T.C., and Watanabe, D.H., 1995, U-Pb ages from the Nimish Formation and Montagnais glomeroporphyritic gabbro of the central New Quebec Orogen, Canada: Canadian Journal of Earth Sciences, v. 32, p. 1208-1220.

Floran, R.J., and Papike, J.J., 1975, Petrology of the low grade rocks of the Gunflint iron formation, Ontario-Minnesota: Geological Society of America Bulletin, v. 86, p. 1169-1190.

Fralick, P.W., 1988, Microbial bioherms, Lower Proterozoic Gunflint Formation, Thunder Bay, Ontario, *in* Geldsetzer, H.H.J., James, N.P., and Tebbutt, G.E., eds., Reefs in Canada and Adjacent Areas: Canadian Society of Petroleum Geologists, Memoir 13, p. 24-29.

Fralick, P.W., 2003, Geochemistry of clastic sedimentary rocks: ratios techniques, *in* D.R. Lentz ed., Geochemistry of Sediments and Sedimentary Rocks: Evolutionary Considerations to Mineral Deposit-Forming Environments, Geological Association of Canada, Geotext 4, p. 85-103.

Fralick, P.W., and Barrett, T.J., 1995, Depositional controls on iron formation associations in Canada, *in* Plint, A.G., ed., Sedimentary Facies Analysis: International Association of Sedimentologists, Special Publication 22, p. 137-156.

Fralick, P.W., Barrett, T.J., Jarvis, K.E., Jarvis, I., Schnieders, B.R., and van de Kemp, R., 1989, Sulfide-facies iron formation at the Archean Morley occurrence, northwestern Ontario: contrasts with ocean hydrothermal deposits: Canadian Mineralogist, v.27, p. 601-616.

Fralick, P.W., Davis, D.W. and Kissin, S.A., 2002. The age of the Gunflint Formation, Ontario, Canada: single zircon U-Pb age determinations from reworked volcanic ash. Canadian Journal of Earth Sciences, v. 39, p. 1085-1091.

Fralick, P.W., Grotzinger J.P., and Edgar, L.A., 2012, Potential recognition of accretionary lapilli in distal impact deposits on Mars: a facies analog provided by the

1.85 Ga Sudbury impact deposit, *in* J.P. Grotzinger and R.E. Milliken, eds., Sedimentary Geology of Mars: SEPM (Society for Sedimentary Geology) Special Publication 102, p. 211-228.

Fralick, P.W., Kissin, S.A., and Davis, D.W., 1998, The age and provenance of the Gunflint Lapilli tuff: Institute on Lake Superior Geology, v. 44, p. 66-67.

Fralick, P.W., and Kronberg, B.I., 1997, Geochemical discrimination of clastic sedimentary rock sources, Sedimentary Geology, v. 113, p. 111-124.

Fralick, P.W., and Riding, R., 2015, Steep Rock Lake: Sedimentology and geochemistry of an Archean carbonate platform: Earth-Science Reviews, v. 151, p. 132-175.

Frei, R., Gaucher, C., Poulton, S.W., and Canfield, D.E., 2009, Fluctuations in Precambrian atmospheric oxygenation recorded by chromium isotopes: Nature, v. 461, p. 250-254.

French, J.E., Heaman, L.M., Chacko, T., and Srivastava, R.J., 2008, Southern Bastar-Cuddapah mafic igneous events, India: A newly recognized large igneous province: Precambrian Research, v. 160, p. 308-322.

Gale, A, Dalton, C.A., Langmuir, C.H., Su, Y., and Schilling, J.-G., 2013, The mean composition of ocean ridge basalts. Geochemistry Geophysics Geosystems, v. 14, p. 489-518.

German, C.R., Hergt, J., Palmer, M.R., and Edmond, J.M., 1999, Geochemistry of a hydrothermal sediment core from the OBS vent-field, 21°N East Pacific Rise: Chemical Geology, v. 155, p. 65-75.

Goodwin, A.M., 1956, Facies relations in the Gunflint iron-formation: Economic Geology, v.51, p. 565-595.

Goodwin, A.M., 1960, Gunflint iron formation of the Whitefish Lake area, District of Thunder Bay: Ontario Department of Mines, Annual Report, v. 61, pt. 7, p. 41-63.

Gordon, T.M., Hunt, P.A., Bailes, A.H., and Syme, E.C., 1990, U-Pb ages from the Flin Flon and Kisseynew Belts, Manitiba: chronology of crust formation at an early Proterozoic accretionary margin, *in* Lowery, J.F., and Stauffer, M.R., eds., The Early Proterozoic Trans-Hudson Orogen of North America: Geological Association of Canada, Special Paper 37, p. 177-199.

Gruau, G., Dia, A., Olivie-Lauquet, G., Davranche, M., and Pinay, G., 2004, Controls on the distribution of rare earth elements in shallow groundwaters: Water Research, v. 38, p. 3576-3586.

Hannigan, R.E., and Sholkovitz, E.R., 2001, The development of middle rare earth element enrichments in freshwater: weathering of phosphate minerals: Chemical Geology, v. 175, p. 495-508.

Hassler, S.W., and Simonson, B.M., 1989, Deposition and alteration of volcaniclastic strata in two large, early Proterozoic iron-formations in Canada: Canadian Journal of Earth Sciences, v. 26, p. 1574-1585.

Heaman, L.M., Machado, N, Krogh, T.E., and Weber, W., 1986, Precise U-Pb zircon ages for the Molson dyke swarm and the Fox River sill; constraints for early Proterozoic crustal evolution in northwestern Manitoba, Canada: Contributions to Minerology and Petrology, v. 94, p. 82-89.

Heaman, L.M., Peck, D., and Toope, K., 2009, Timing and geochemistry of 1.88 Ga Molson igneous events, Manitoba: insights into the formation of a craton-scale magmatic and metallogenic province: Precambrian Research, v. 172, p. 143-162.

Hemming, S.R., McLennan, S.M., and Hanson, G.N., 1995. Geochemical and Nd/Pb isotopic evidence for the provenance of the Early Proterozoic Virginia Formation, Minnesota. Implications for the tectonic setting of the Animikie Basin. Journal of Geology, v. 103, p. 147-168.

Hill, M.L., and Smyk, M.C., 2005, Penokean fold-and-thrust deformation and the Paleoproterozoic Gunflint Formation near Thunder Bay, Ontario: Institute on Lake Superior Geology, v. 51, p. 26.

Hoffman, P.F., 1987. Early Proterozoic foredeeps, foredeep magmatism, and superior-type iron formations of the Canadian Shield. *In*, Proterozoic Lithospheric Evolution. Ed. A. Kroner, American Geophysical Union, Geodynamics Series, 17, p. 85-98.

Holland, H.D., 2005, Sedimentary mineral deposits and the evolution of the Earth's near-surface environments: Economic Geology, v. 100, p. 1489-1509.

Holser, W.T., 1997, Evaluation of the application of rare-earth elements to paleoceanography: Palaeogeography, Palaeoclimatology, Paleoecology, v. 132, p. 309-323.

Hostetler, P.B., and Garrels, R.M., 1962, Transportation and precipitation of uranium and vanadium at low temperatures, with special reference to sandstone-type uranium deposits: Economic Geology, v. 57, p. 137-152.

Hulbert, L.J., Hamilton, M.A., Horan, M.F., and Scoates, R.F.J., 2005, U-Pb and Re-Os isotope geochronology of mineralized ultramafic intrusions and associated nickel ores from the Thompson nickel belt, Manitoba, Canada: Economic Geology, v.100, p. 29-41.

James, N.P., and Choquette, P.W., 1990, Limestones – the meteoric diagenetic environment, *in* MacIlreath, I.A., and Morrow, D.W., eds., Diagenesis. Geoscience Canada, Reprint Series 4, p. 35-74.

Jacobsen, S.B., and Pimentel-Klose, M.R., 1988, Neodymium isotopic variations in Precambrian banded iron formations: Geophysical Research Letters, v. 15/4, p. 393-396.

Ji, H., Wang, S., Ouyang, Z., Zhang, S., Sun, C., Liu, X., and Zhou, D., 2004, Geochemistry of red residua underlying dolomites in karst terrains of Yunnan-Guizhou Plateau II: the mobility of rare earth elements during weathering: Chemical Geology, v. 203, p. 29-50.

Jirsa, M.A., 2008, Scientists unearth ancient impact's secrets: Astronomy, v. 36, issue 12, p. 32-37

Johnson, T.M., and Bullen, T.D. 2004, Mass-dependent fractionation of selenium and chromium isotopes in low-temperature environments: Geochemistry of Non-Traditional Stable Isotopes, v. 55, p. 289-317.

Johnston, D.T., Poulton, S.W., Fralick, P.W., Wing, B.A., Canfield, D.E., and Farquhar, J., 2006, Evolution of the ocean sulfur cycle at the end of the Paleoproterozoic: Geochimica et Cosmochimica Acta, v. 70, p. 5723-5739.

Jones, C., Nomosatryo, S. Cerowe, S.A, Bjerrum, C.J. and Canfield, D.E., 2015, Iron oxides, divalent cations, silica and the early Earth: Geology, v. 43, p. 135-138.

Kamber, B.S., and Webb, G.E., 2001. The geochemistry of Late Archean microbial carbonate: implications for ocean chemistry and continental erosion. Geochimica et Cosmochimica Acta, v. 65, p. 2509-2525.

Kamber, B.S., Bolhar, R., and Webb, G.E., 2004, Geochemistry of late Archean stromatolites from Zimbabwe: evidence for microbial life in restricted epicontinental seas: Precambrian Research, v. 132, p. 379-399.

Kissin, S.A., and Fralick, P.W., 1994. Early Proterozoic volcanics of the Animilie Group, Ontario and Michigan, and their tecyonic significance. Proceedings of the Institute on Lake Superior Geology, v. 40, p. 18-19.

Kissin, S.A., Vallina, D.A., Addison, W.D., and Brumpton, G.R., 2003, New zircon ages from the Gunflint and Rove Formations, northwestern Ontario: Institute on Lake Superior Geology, v. 49, p. 43-44.

Klasner, J.S., Ojakangas, R.W., Schulz, K.J., and LaBerge, G.L., 1991. Nature and style of deformation in the foreland of the Early Proterozoic Penokean Orogeny, northern Michigan. United States Geological Survey, Bulletin 1904K.

Koppi, A.J., Edis, R., Field, D.J., Geering, H.R., Klessa, D.A., and Cockayne, J.H., 1996, Rare earth element trends and cerium-uranium-manganese associations in weathered rock from Koongarra, Northern Territory, Australia: Geochimica et Cosmochimica Acta, v. 60, p. 1695-1707.

Krogh, T.E., Davis, D.W., and Corfu, F., 1984, Precise U-Pb zircon and baddeleyite ages for the Sudbury area, *in* Pye, E.G., ed., The Geology and Ore Deposits of the Sudbury Structure: Ontario Geological Survey, Special Volume 1, p. 431-446.

Land, L.S., 1970, Phreatic versus vadose meteoric diagenesis of limestones: evidence from a fossil water table: Sedimentology, v. 14, p. 175-185.

Lei, W., Linsalata, P., Franca, E.P., and Eisenbud, M., 1986, Distribution and mobilization of cerium, lanthanum and neodymium in the Morro do Ferro basin, Brazil: Chemical Geology, v. 55, p. 313-322.

Lewan, M.D., and Maynard, J.B., 1982, Factors controlling enrichment of vanadium and nickel in the bitumen of organic sedimentary rocks: Geochimica et Cosmochimica Acta., v. 46, p. 2547-2560.

Liu, Y.-G., Miah, M.R.U., and Schmitt, R.a., 1988, Cerium: a chemical tracer for paleo-oceanic redox conditions: Geochimica et Cosmochimica Acta, v. 52, p. 1361-1371.

Maric, M., and Fralick, P.W., 2005, Sedimentology of the Rove and Virginia Formations and their tectonic significance: Institute on Lake Superior Geology, v. 51, p. 41-42.

Marsh, J.S., 1991, REE fractionation and Ce anomalies in weathered Karoo dolerite: Chemical Geology, v. 90, p. 189-194.

Meert, J.L., Pandit, M.K., Pradham, V.R., and Kamenov, G., 2011. Preliminary report on the paleomagnetism of 1.88 Ga dykes from the Bastar and Dharwar cratons, peninsular India: Gondwana Research, v. 20, p. 335-343.

Michard, A., Michard, G., Stuben, D., Stoffers, P., Cheminee, J.-L., and Binard, N., 1993, Submarine thermal springs associated with young volcanoes: the Teahitia vents, Society Islands, Pacific Ocean: Geochimica et Cosmochimica Acta, v. 57, p. 4977-4986.

Morey, G.B., 1967. Stratigraphy and sedimentology of the middle Precambrian Rove Formation in northeastern Minnesota. Journal of sedimentary petrology, v. 37, p. 1154-1162.

Morey, G.B., 1969. The geology of the Middle Precambrian Rove Formation in northeastern Minnesota. Minnesota Geological Survey, SP-7, 62p.

Morey, G.B., and Southwick, D.L., 1995. Allostratigraphic relationships of the early Proterozoic iron-formations in the Lake Superior Region. Economic Geology, v. 90, p. 1983-1993.

Murray, R.W., Buchholtz ten Brink, M.R., Jones, D.L., Gerlach, D.C., and Russ, G.P., 1990, Rare earth elements as indicators of different marine depositional environments in chert and shale: Geology, v. 18, p. 268-271.

Northrop, H.R., and Goldhaber, M.B., 1990, Genesis of the tabular-type vanadium-uranium deposits of the Henry Basin, Utah: Economic Geology, v. 85, p. 215-269.

Ohta, A., and Kawabe, I., 2001, REE (III) adsorption onto Mn dioxide and Fe oxyhydroxide: Ce (III) oxidation by Mn dioxide: Geochimica et Cosmochimica Acta, v. 65, p. 695-703.

Ojakangas, R.W., 1983, Tidal deposits in the early Proterozoic basin of the Lake Superior region – the Palms and Pokegama Formations: evidence for subtidal-shelf deposition of Superior type banded iron formations, *in* Medaris, L.G., ed., Early Proterozoic Geology of the Great Lakes Region: Geological Society of America, Memoir 160, p. 49-66.

Oze, C., Bird, D.K., and Fendorf, S., 2007, Genesis of hexavalent chromium from natural sources in soil and groundwater: Proceedings of the National Academy of Science, v. 104, p. 6544-6549.

Pan, Y., and Stauffer, M.R., 2000, Cerium anomaly and Th/U fractionation in the 1.85 Ga Flin Flon paleosol; clues from REE- and U-rich accessory minerals and implications for paleoatmospheric reconstruction: American Mineralogist, v. 85, p. 898-911.

Partin, C.A., Bekker, A., Planavsky, N.J., Scott, C.T., Gill, C., Li, C., and Podkovyroy, V., 2013, Large-scale fluctuations in Precambrian atmospheric and oceanic oxygen levels from the record of U in shales: Earth and Planetary Science Letters, v. 369, p. 284-293.

Poulton, S.W., Fralick, P.W., and Canfield, D.E., 2004, The transition to a sulfidic ocean 1.84 billion years ago: Nature, v. 431, p. 173-177.

Poulton, S.W., Fralick, P.W., and Canfield, D.E., 2010, Spatial variability in oceanic redox structure 1.8 billion years ago: Nature Geoscience, v. 3, p. 486-490.

Planavsky, N.J., Bekker, A., Heffman, A., Owens, J.D., and Lyons, T.W., 2012, Sulfur record of rising and falling marine oxygen and sulfate levels during the Lomagundi event: Proceedings of the National Academy of Science, v. 109, p. 18300-18305.

Planavski, N.J., Bekker, A., Rouxel, O., Kamber, B., Hofmann, A., Knudsen, A., and Lyons, T.W., 2010. Rare earth element and yttrium compositions of Archean and Paleoproterozoic Feformations revisited: New perspectives on the significance and mechanisms of deposition. Geochimica et Cosmochimica Acta, v. 74, p. 6387-6405.

Planavsky, N.J., Rouxel, O., Bekker, A., Shapiro, R., Fralick, P.W., and Knudsen, A., 2009, Iron-oxidizing microbial ecosystems thrived in late Paleoproterozoic redox-stratified oceans: Earth and Planetary Science Letters, v. 286, p. 230-242.

Planavsky, N.J., et al. 2014, Low Mid-Proterozoic atmospheric oxygen levels and the delayed rise of animals: Science, v. 346, p. 635-638.

Premovic, P.I., Premovic, M.S., and Pavlovic, N.Z., 1986, Vanadium in ancient sedimentary rocks of marine origin: Geochimica et Cosmochimica Acta, v. 50, p. 1923-1931.

Pufahl, P.K., and Fralick, P.W., 2004, Depositional controls on Paleoproterozoic shallow water iron formation accumulation, Gogebic Range, Wisconsin, U.S.A.: Sedimentology, v. 54, p. 791-808.

Pufahl, P.K., Hiatt, E.E., Stanley, C.R., Morrow, J.R., Nelson, G.J., and Edwards, C.T., 2007, Physical and chemical evidence of the 1850 Ma Sudbury impact event in the Baraga Group, Michigan: Geology, v. 35, p. 827-830.

Rankin, P.C., and Childs, C.W., 1976, Rare-earth elements in iron-manganese concretions from some New Zealand soils: Chemical Geology, v. 18, p. 55-64.

Rasmussen, B., Fletcher, I.R., Bekker, A., Muhling, J.R., Gregory, C.J., and Thorne, A.M., 2012, 1.88Ga iron formations signal return to iron-rich oceans coeval with rapid crustal growth: Nature, v. 484, p. 498-501.

Reinhard, C.T., et al. 2014, The isotopic composition of authigenic chromium in anoxic marine sediments: A case study from the Cariaco Basin: Earth and Planetary Science Letters, v. 407, p. 9-18.

Richard, L.R., 1997, REE normalizing values for average seawater: Minpet: Mineralogical and Petrological Data Processing System. Commercial computer program.

Ricketts, B.D., Ware, M.J., and Donaldson, J.A., 1982, Volcaniclastic rocks and volcaniclastic facies in the middle Precambrian Belcher Group, Northwest Territories, Canada: Canadian Journal of Earth Sciences, v. 19, p. 1275-1294.

Riding, R., Fralick, P.W., and Liang, L., 2014, Identification of an Archean marine oxygen oasis: Precambrian Research, v. 251, p. 232-237.

Roscoe, S.M., 1969, Huronian rocks and uraniferous conglomerates in the Canadian Shield: Geological Survey of Canada Paper 68-40, 205 p.

Schauble, E.A., Rossman, G.R., and Taylor, H.P.J., 2004, Theoretical estimates of equilibrium chromium-isotope fractionations: Chemical Geology, v. 205, p. 99-114.

Scheiderich, K., Amini, M., Holmden, C., and Francois, R., 2015. Global variability of chromium isotopes in seawater demonstrated by Pacific, Atlantic and Arctic Ocean samples. Earth and Planetary Science Letters, v. 423, p. 87-97.

Schneider,D.A., Bickford, M.E., Cannon, W.F., Schulz, K.J., and Hamilton, M.A., 2002, Age of volcanic rocks and syndepositional iron formations, Marquette Range Supergroup; implications for the tectonic setting of Paleoproterozoic iron formations of the Lake Superior region: Canadian Journal of Earth Sciences, v. 39, p. 999-1012.-MS: Chemical Geology, v. 249, p. 294-306.

Schoenberg, R., Zink, S., Staubwasser, M., and von Blanckenburg, F., 2008, The stable Cr isotope inventory of solid Earth reservoirs determined by double spike MC-ICP

Schulz, K.J., and Cannon, W.F., 2007, The Penokean Orogeny in the Lake Superior region: Precambrian Research, v. 157, p. 4-25.

Shiller, A.M., and Mao, L., 1999, Dissolved vanadium on the Louisiana shelf: effect of oxygen depletion: Continental Shelf Research, v. 19, p. 1007-1020.

Shiller, A.M., and Mao, L., 2000, Dissolved vanadium in rivers: effects of silicate weathering: Chemical Geology, v. 165, p. 13-22.

Sholkovitz, E.R., 1995, The aquatic chemistry of rare earth elements in rivers and estuaries: Aquatic Geochemistry, v. 1, p. 1-34.

Simonson, B.M., and Goode, A.D.T., 1989, First discovery of ferruginous chert arenites in the early Precambrian Hamersley Group of Western Australia: Geology, v.17, p. 269-272.

Sims, P.K., Van Schmus, W.R., Schulz, K.J., and Peterman, Z.E., 1989, Tectonostratigraphic evolution of the Early Proterozoic Wisconsin magmatic terranes of the Penokean orogen: Canadian Journal of Earth Science. v. 26, p. 2145-2158.

Slack, J.F., and Cannon, W.F., 2009, Extraterrestrial demise of banded iron formations 1.85 billion years ago: Geology, v. 37, p. 1011-1014.

Smedley, P.L., 1991, The geochemistry of rare earth elements in groundwater from the Carnmennellis area, southwest England: Geochimica et Cosmochimica Acta, v. 55, p. 2767-2779.

Southwick, D.L., and Morey, G.B., 1991. Tectonic imbrication and foredeep development in the Penokean Orogeny, east-central Minnesota – an interpretation based on regional geophysics and the results of test-drilling. United States Geological Survey, Bulletin 1904C.

Spray, J.G., Butler, H.R., and Thompson, L.M., 2004, Tectonic influences on the morphology of the Sudbury impact structure: Implications for terrestrial cratering and modeling: Meteoritics and Planetary Science, v. 39, p. 287-301.

Sugiyama, M., 1989, Seasonal variation of vanadium concentration in Lake Biwa, Japan: Geochemistry Journal, v. 23, p. 111-116.

Sumner, D.Y., 1997, Carbonate precipitation and oxygen stratification in late Archean seawater as deduced from facies and stratigraphy of the Gamohaan and Frisco formations, Transvaal Supergroup, South Africa: American Journal of Science, v. 297, p. 455-487.

Sumner, D.Y., and Grotzinger, J.P., 2000, Were kinetics of calcium carbonate precipitation related to oxygen concentration?: Geology, v. 24, p. 119-122.

Sverjensky, D.A., 1984, Europium redox equilibria in aqueous solution: Earth and Planetary Science Letters, v. 67, p. 70-78.

Taylor, S.R., and McLennan, S.M., 1985. The Continental Crust: Its Composition and Evolution; an Examination of the Geochemical Record Preserved in Sedimentary Rocks: Blackwell, Oxford, 312 pp.

Thompson, M., and Walsh, J.N., 1989, Inductively Coupled Plasma Spectrometry: Chapman and Hill, New York, 315 p.

Thorstenson, D.C., MacKenzie, F.T., and Ristvet, B.L., 1972, Experimental vadose and phreatic cementation of skeletal carbonate sand: Journal of Sedimentary Petrology, v. 42, p. 162-167.

Tomlinson, K.Y., 1999, Project Unit 95-027; refinement of hafnium (Hf) and zirconium (Zr) ICP-MS analyses by improvements in the sample digestion procedure: Ontario Geological Survey Miscellaneous Paper 1999, p. 189-192.

Van Wyck, N., and Johnson, C.M., 1997. Common lead, Sm-Nd, and U-Pb constraints on petrogenesis, crustal architecture and tectonic setting of the Penokean Orogen (Paleoproterozoic) in Wisconsin, USA. Geological Society of America Bulletin, v. 109, p. 799-808.

Wanty, R.B., and Goldhaber, M.B., 1992, Thermodynamics and kinematics of reactions involving vanadium in natural systems: accumulation of vanadium in sedimentary rocks: Geochimica et Cosmochimica Acta, v. 56, p. 1471-1483.

Webb, G.E., and Kamber, B.S., 2000, Rare earth elements in Holocene reefal microbialites: a new shallow seawater proxy: Geochimica et Cosmochimica Acta, v.64, p. 1557-1565.

Webb, G.E., Northdurft, L.K., Kamber, B.S., Kloprogge,J.T., and Zhaos, J.-Z., 2009, Rare earth element geochemistry of scleractinian coral skeleton during meteoric diagenesis: a sequence through neomorphism of aragonite to calcite: Sedimentology, v. 56, p. 1433-1463.

Wehrli, B., and Stumm, W., 1989, Vanadyl in natural waters: adsorption and hydrolysis promote oxygenation: Geochimica et Cosmochimica Acta, v. 53, p. 69-77.

Wright, J., Schrader, H., and Holser, W.T., 1987, Paleoredox variations in ancient oceans recorded by rare earth elements in fossil apatite: Geochimica et Cosmochimica Acta, v. 51, p. 631-644.

Yang, J., Sun, W., Wang, Z., Xue, Y., and Tao, X., 1999, Variations in Sr and C isotopes and Ce anomalies in successions from China: evidence for the oxygenation of Neoproterozoic seawater: Precambrian Research, v. 93, p. 215-233.

Zbinden, E.A., Holland, H.D., Feakes, C.R. and Dobos, S.K., 1988, The Sturgeon Falls Paleosol and the Composition of the Atmosphere 1.1 Ga Bp: Precambrian Res, v. 42, p. 141-163.

Zhong, S., and Mucci, A., 1995, Partitioning of rare earth elements (REEs) between calcite and seawater solutions at 25°C and 1atm and high dissolved REE concentrations: Geochimica et Cosmochimica Acta, v. 58, p. 443-453.

Zink, S., Schoenberg, R., and Staubwasser, M., 2010, Isotopic fractionation and reaction kinetics between Cr(III) and Cr(VI) in aqueous media: Geochemica et Cosmochimica Acta, v. 74, p. 5729-5745.

FIGURE CAPTIONS

Figure 1. A) Location of rocks deposited in the Animikie basin. Geological sketch map of the western Lake Superior region showing distribution of the Paleoproterozoic Animikie Group and Archean terrains. The main iron formation bearing sedimentary units are shown in black (Gunflint, Mesabi, Cuyuna, Gogebic, Iron River and Marquette). B) Locations of main areas of study (black circles 1 to 5) of the Gunflint Formation in the Thunder Bay area.

Figure 2. Stratigraphy of the Gunflint Formation with the area at the top of the formation enlarged. The ankerite grainstones directly underlying the limestone are silicified. The limestone is erosively overlain by the impact layer from the Sudbury impact event. At some locations the impact layer is overlain by ankerite grainstones, which are in turn erosively overlain by siltstones of the Rove Formation. Regressive exposure surfaces exist above silicified areas and at the tops of coarsening upward successions. The lower

member of the Gunflint Formation extends from the base to the exposure surface at the top of the silicified layer approximately 50 m above the base. The upper member extends from there to the base of the limestone.

Figure 3. Rock outcrop at Area 1. A) *In situ* stromatolites of the Limestone Member underlying boulder conglomerate (not seen in photo) created by the Sudbury impact event (bedding-plane view). Fine-grained grainstone (pale grey) is banked up against the stromatolites. In places, channels are eroded into the fine grainstone between stromatolitic mounds and filled with the otherwise overlying coarse grainstone (arrow). B) Reflected light photomicrograph of coarse grainstone composed of coarse- to very coarse-grained sand, granules and small pebbles, which mostly contain chlorite, and stromatolite fragments. White calcite cement fills interstitial areas. Graded fine- to very fine-grained sand bed with calcite cement overlies the coarse layer. C) Layering in a stromatolite. The medium-grey material is chlorite with calcite and the white cement is calcite (photomicrograph of thin section taken in reflected light.). D) Sudbury impact boulder conglomerate stratigraphically above an erosive surface cut into the underlying calcitic grainstones and stromatolites. The clasts of originally underlying ankeritic grainstone and limestone were lithified prior to erosion. E) The matrix of the Sudbury impact conglomerate showing amygdaloidal, devitrified glass, and rock fragments derived from underlying strata, encased in fine-grained ankerite. Other areas contain blocky calcite cement instead of the ankerite.

Figure 4. Rock outcrop at Area 2. A) Sudbury impact boulder conglomerate containing clasts of calcitic grainstone, ankeritic grainstone and black chert. A boulder is highlighted by the dashed line. B) A large, overturned rectangular slab consisting of calcitic grainstones and stromatolites. An upside-down stromatolite with a surficial hematite stain is to the right of the scale card (arrow). C) A fragment of a calcitic stromatolite within the impact boulder conglomerate. D) An area of the impact conglomerate with devitrified glass, black chert granules and prominent blocky calcite cement.

Figure 5. Rock outcrop at Area 3. A) Stromatolite overlain by a coarse-grained grainstone; from an *in situ* exposure directly underlying the Sudbury impact layer with accretionary lapilli and rarer boulders and cobbles. B) Impact accretionary lapilli with a matrix composed of devitrified glass and calcite cement. At most exposures in this outcrop the impact layer erosively overlies the calcitic stromatolites and grainstones (lower half of image).

Figure 6. Ankeritic grainstone at Area 4. A) Cross-sectional view of a cross-stratified tempestite resting on the silicified top of the underlying bed (where the coin is). Its hummocky top has been silicified. B) Plan view of medium-grained ankeritic grainstone with rip-up clasts of silicified stromatolite and grainstone.

Figure 7. Thin-section photomicrographs (in cross-polarized light XPL) of calcareous grainstone and stromatolite samples. A) A sample from the lower coarse grainstone layer from Area 1 showing angular fragments containing chlorite in blocky calcite cement.

Clasts in the coarse grainstones commonly range from 0.5 to 5 mm. The calcite cement can be seen overgrowing the internal structure of some grains (arrow) and also scalloping their edges in places (left of arrow). B) A sample from the upper coarse grainstone, Area 1, composed of grains containing chlorite (black) and stromatolitic fragments with blocky calcite cement (cal., light grey) containing siliceous cements (sil., white) filling dissolution channel-ways (XPL). C) Grainstone composed of chlorite and stromatolitic fragments with siliceous cements filling dissolution channel-ways through the blocky calcite cement (arrow). The sample is from the upper grainstone layer of an inverted boulder at Area 2. The lower grainstone, which is now on the top surface of the inverted boulder, is much less altered, indicating that formation of channel-ways and silica cement occurred prior to inversion (XPL). D) Stromatolitic layering in a large, inverted slab at Area 2. Alternating layers are rich in chlorite or blocky calcite cement. Note again that the amount of silica replacement decreases from the original top of the block (C) to the original base of the inverted block (D).

Figure 8. SEM backscatter electron image and x-ray geochemical analyses of a coarse grainstone from Area 1. Chlorite grains (e.g. points 1 and 6) and chlorite and calcite stromatolitic fragments (e.g. points 2 and 3, respectively) occur in calcite cement (e.g. point 5). Note the high MnO content of the cement, especially in contrast to FeO, which is below detection and the consistently high vanadium values in the chlorite (analyses 1, 2 and 6). The very dark areas are quartz.

Figure 9. Agate veins developed in the Sudbury ejecta layer near Area 1. An open space contains miniature stalactites indicating formation of these silicious deposits in the vadose zone. The grey portion of the stalactites represents the material that formed in the vadose zone. The isopachous layer of white chert covering the grey stalactites and bottom of the cavity probably formed in the phreatic zone. The dark material in the chert at the bottom of the vug may represent vadose silt. This style of siliceous veins is only present in the ejecta layer and more rarely in the underlying limestone. The formation of these types of vug fills clearly shows the meteoric nature of the cements.

Figure 10. Scatter-plots depicting concentrations of V, Cr, U, P_2O_5 and Ce in carbonates of the upper Gunflint and ejecta layer. A) Cr and especially V are enriched in the coarse grainstones and stromatolites of the Limestone member and the matrix and calcite cement in the ejecta layer. The fine grainstone is enriched in V but less so in Cr. B) U has higher concentrations in the Limestone member and ejecta matrix than most of the ankerite samples. (Fewer points are plotted on this graph due to small sample size precluding ICP-MS analyses on some samples.) C) The coarse grainstones and stromatolites have the largest concentrations of P_2O_5. The fine grainstones and ejecta matrix/cements have intermediate values and the ankeritic grainstones have the lowest concentrations. D) Pr/Pr* was used to represent the Ce anomaly and was calculated as Pr/Pr*=Pr/(.5Ce+.5Nd) after all had been normalized by dividing by values for post Archean Australian shale (PAAS) (Taylor and McLennan, 1985). The formula Ce/Ce*=Ce/(.5La+.5Pr) should not be used to calculate Ce anomalies for Archean and Paleoproterozoic chemical sediments as these rocks commonly have La anomalies, which

will lead to false negative Ce anomalies if Ce/Ce* is used (see Bau and Dulski (1996) for further explanation of rational). Numbers above one indicate increasing negative anomaly and numbers below one increasing positive anomaly. The Limestone member and ejecta samples have significant negative anomalies, whereas the ankeritic grainstones have no anomaly to significant positive anomalies.

Figure 11. Ratio scatterplots of Al_2O_3, V, Cr and P_2O_5. The concentration of Al_2O_3 corresponds to the amount of siliciclastics (mainly chlorite) in the samples. If another element in the carbonate samples is primarily in the siliciclastic portion it will plot with a consistent element/Al_2O_3 ratio (Fralick and Kronberg, 1997; Fralick 2003). Thus, if the V, Cr and P_2O_5 were primarily in the siliciclastic detritus all points would plot in a tight cluster. This is not the case as the stromatolites, ankerite and calcite grainstones, and impact conglomerate matrix from linear arrays with a large amount of variation in the elemental ratios. The fine-grained calcite grainstones are deficient in Cr compared to the Cr/Al_2O_3 ratio of other samples and this may be a result of their larger content of siliciclastic material. For comparison average mid-ocean ridge basalt has V/Al_2O_3=21 and Cr/Al_2O_3=17 (Gale et al., 2013).

Figure 12. Rare earth element patterns of samples from the limestone unit, matrix of the overlying impact produced conglomerate (A, B and C), and Gunflint ankerite grainstones (D); normalized using Post Archean Australian Shale (Taylor and McLennan, 1985). The calcite stromatolites, coarse grainstones and fine grainstones all have pronounced negative Ce anomalies with generally hat-shaped patterns (middle rare earth element

enrichment). In modern systems these patterns have been interpreted to reflect oxic conditions and precipitation from non-marine waters where weathering of phosphate minerals enriched the middle REEs relative to shale (Hannigan and Sholkovitz, 2001). The REE patterns of the ankerite grainstone samples are very different from the limestone samples. They have pronounced positive Eu anomalies and small positive Ce anomalies, with slightly enriched to slightly depleted heavy REEs. The cause of the large positive La anomalies in some samples is unknown. The REE patterns for the samples of conglomerate matrix are intermediate between the calcite and ankerite samples.

Figure 13. PAAS normalized Eu anomaly, Eu/Eu*=Eu/(0.66Sm+0.33Tb), plotted against PAAS normalized Pr anomaly, Pr/Pr*=Pr/(.5Ce+.5Nd) used as a proxy for the Ce anomaly (see Methods). The ankerite grainstone samples have distinct positive Eu anomalies and very minor to large positive Ce anomalies. The limestone samples have large negative Ce anomalies and generally small positive Eu anomalies. The latter are consistent with middle rare earth element enrichment and imply that the limestones were not precipitated from Gunflint Sea marine water. One stromatolite sample has a significant positive Eu anomaly that may have been caused by a period of upward circulating groundwater bringing dissolved REEs from the ankerite grainstone. The conglomerate matrix is intermediate between the limestone and ankerite.

Figure 14. Scatterplot of δ^{53}Cr (‰) against Cr/Ti. The Cr/Ti ratio for the ankerite grainstones and two of the impact conglomerate matrixes are similar and probably reflect the ratio of the source siliciclastic material. In contrast, the calcite-rich coarse grainstones

and stromatolites are enriched in Cr and the fine-grained calcite grainstones are depleted. Two of the ankerite grainstones and the fine-grained calcite grainstones have crustal values of δ^{53}Cr. The other samples are enriched in the heavy isotope. Legend as in Figure 10.

Figure 15. Trends in the concentration of vanadium (ppm) in five drill holes located on a line obliquely crossing the Gunflint shelf. Each hole comprises a complete section through the Biwabik or Gunflint iron formation; columns are hung from the top of the Formation. The 162 samples used to construct this cross-section were collected as grainstone – fine-grained chemical sediment pairs of samples. The higher value of each of these sample pairs was used to construct this diagram. The lower anomaly at 50 meters occurs directly below a regression surface with subaerial exposure in the north. The upper, pronounced positive anomaly increases towards the top of the formation where there are exposure surfaces both below and above the limestone unit at the top of the Gunflint Formation.

Figure 16. Comparison between the REE pattern for a typical Gunflint calcite grainstone and modern groundwater. The groundwater REE patterns are for samples from a catchment in western France (Gruau et al., 2004) where both shallow, upland oxygenated groundwater and shallow wetland groundwater with a low redox potential were analyzed. Middle REE enrichment occurs in all three samples, but only O_2-rich groundwater samples had the negative Ce anomalies (Gruau et al., 2004) comparable to the limestone samples of this study. The REE concentrations of the modern water samples are in nmol/l

and the values for the upland water were multiplied by 100. The Tm and Lu values for the upland water were extrapolated from the trend of adjacent elements as the original data was missing.

Figure 17. Block diagrams depicting deposition and modification of the rocks studied. A) Hummocky and trough cross-stratified ankerite grainstones deposited prior to maximum regression and sub-aerial exposure (area at top of block diagram). These ankerite grainstones and near-shore stromatolites represent site 4A on Figure 2 located approximately 50 m above the Archean basement. B) Upon exposure ankerite grainstones in the uppermost Gunflint Formation were silicified (S) and overlain by calcite grainstones and stromatolites of the Limestone member, which were deposited in a non-marine environment. The chlorite-bearing layers in the stromatolites were probably formed from mafic volcanic ash that stuck to their surface. C) The calcite grainstones and stromatolites were overlain by volcanic ash and underwent meteoric diagenesis in the vadose and phreatic zones, which produced blocky calcite cements. D) The Sudbury impact event created seismic waves that shattered the lithified grainstones and microbialites. The debris was redeposited by the blast-cloud from the impact and mixed with accretionary lapilli and melt fragments (Addison et al., 2010; Fralick et al., 2012). Non-marine calcite cements formed in the debris from phreatic zone groundwater, while small silica stalactites developed in open spaces in the vadose zone.

TABLE 1. Whole Rock Geochemistry

Samples are: Calcite Stromatolite, Coarse and Fine Calcite Grainstone, Matrix of Impact Conglomerate and Ankerite Grainstone

	SITE 1				SITE 2					SITE 3				
	Strom.	Coarse	Fine	Cong.	Coarse		Fine	Cong.		Strom.	Coarse	Cong.	Ankerite Grainstor	
	G-3A	G3b-Y	G-3b-X	06-2	06-20A	06-21	06-22	06-24	06-23	06-12B	06-12A	06-30	CR-1B	CR-2A
SiO_2	N.D.	N.D.	N.D.	32.19	15.6	23.3	10.3	15.3	17.4	12.5	16.6	21.6	18.8	14.2
TiO_2	0.06	0.07	0.30	0.23	0.07	0.02	0.28	0.13	0.10	0.05	0.07	0.10	0.01	0.01
Al_2O_3	2.92	3.82	4.99	6.82	3.74	1.50	5.97	3.10	2.78	1.92	2.58	2.73	0.24	0.40
$Fe_2O_3^+$	7.17	6.94	7.72	6.35	9.51	2.98	10.5	9.64	6.60	4.58	4.23	5.98	10.1	10.3
MnO	0.18	0.36	0.22	0.11	0.33	0.74	0.21	0.31	0.24	0.35	0.39	0.28	0.51	0.48
MgO	2.04	1.97	2.56	2.94	3.99	3.08	4.07	11.9	3.69	11.78	10.6	11.4	10.5	11.0
CaO	43.1	38.5	42.0	25.7	34.5	36.4	36.6	25.2	36.1	30.27	28.9	25.0	19.1	20.5
Na_2O	0.93	0.87	0.76	B.D.	0.03	B.D.	B.D.	0.04	0.02	0.06	0.09	0.05	0.25	0.42
K_2O	0.02	0.02	0.09	1.09	B.D.	0.01	0.02	0.01	0.01	0.47	0.73	0.17	0.05	0.02
P_2O_5	0.15	0.63	0.09	0.07	0.96	0.72	0.17	0.10	0.46	0.26	0.93	0.06	0.01	0.02
LOI	36.3	N.D.	N.D.	23.4	31.1	31.0	31.7	34.1	32.1	37.2	34.4	32.5	40.4	42.7
Y	73	86	33	18	167	102	31.9	14.4	46.8	85	120	11.8	5.13	2.24
La	37.4	34.5	29.5	13.1	94.9	52.6	21.3	11.8	26.1	56.3	67.2	15.5	2.60	1.61
Ce	31.0	37.4	24.2	22.6	113	65.7	25.8	18.1	38.5	52.7	78.0	27.4	5.83	3.94
Pr	6.77	9.85	4.60	2.83	23.6	13.6	4.38	2.32	6.56	9.89	16.7	3.21	0.50	0.37
Nd	30.0	49.0	20.4	10.6	100	60.8	17.5	8.83	28.8	40.1	75.4	11.7	2.02	1.38
Sm	5.54	10.1	4.20	1.98	20.4	12.6	3.09	1.58	5.89	7.34	15.5	2.11	0.41	0.29
Eu	2.14	2.37	1.03	0.55	4.77	3.18	0.71	0.43	1.56	1.77	3.75	0.52	0.13	0.089
Gd	7.24	11.3	4.96	1.96	20	14.4	3.33	1.62	6.59	8.77	18.3	1.93	0.50	0.30
Tb	1.17	1.62	0.90	0.30	3.01	1.95	0.49	0.23	0.88	1.23	2.45	0.28	0.071	0.045
Dy	7.59	9.49	5.91	1.99	17.9	11.6	3.26	1.50	5.18	8.00	14.6	1.65	0.47	0.27
Ho	1.79	1.95	1.42	0.45	3.75	2.45	0.79	0.33	1.07	1.84	3.08	0.34	0.11	0.058
Er	5.18	5.13	4.21	1.34	9.86	6.57	2.56	0.95	2.85	5.38	8.10	0.99	0.31	0.16
Tm	0.72	0.61	0.61	0.18	1.15	0.77	0.37	0.12	0.34	0.70	0.93	0.14	0.044	0.020
Yb	3.46	2.49	3.01	1.02	5.86	4.02	2.23	0.69	1.78	3.90	4.82	0.92	0.27	0.097
Lu	0.49	0.33	0.43	0.14	0.75	0.51	0.32	0.10	0.24	0.53	0.63	0.14	0.037	0.017
Ba	96	77	41	78	37	46	39	108	46	247	338	59	10	10
Cr	110	92	6	78	114	39	8	40	70	123	89	38	B.D.	3
Cu	8	7	16	8	12	8	17	5	12	7	7	26	3	1
Hf	N.D.	N.D.	N.D.	ND	0.7	0.3	1.3	1.0	0.90	0.6	0.9	0.8	B.D.	B.D.
Nb	13	15	7	12	0.8	0.7	3	5.5	3.2	0.4	0.8	3.7	0.4	0.5
Rb	N.D.	N.D.	N.D.	67	0.3	0.6	0.4	0.9	0.6	35	47	7	0.5	0.5
Sr	257	266	151	102	177	375	107	75	142	299	357	135	80	122
Ta	N.D.	N.D.	N.D.	ND	B.D.	B.D.	B.D.	0.4	B.D.	B.D.	B.D.	0.2	B.D.	B.D.
Th	N.D.	0.18	N.D.	8	4	5	1.3	2.5	1.7	0.2	0.7	2	0.1	0.2
U	N.D.	9.3	N.D.	4	19	8.8	10	11	17	14	20	4	4	0.4
V	1330	1520	57	162	1370	684	491	159	588	1242	1240	119	7	6
Zn	38	24	24	79	125	28	48	44	31	39	26	35	10	8
Zr	73	82	89	70	29	16	48	29	36	26	36	30	B.D.	B.D.

N.D. = Not Determined, B.D. = Below Detection

	SITE 1 Stromatolite		Coarse Grainstone						Fine Gst.	SITE 2 Stromatolite		Coarse Grainsto	
	G3Aa	**G3Ab**	**4HaT**	**4HaB**	**4HbT**	**4HbB**	**H3-la**	**H3-1b**	**H-Fine**	**6Ma**	**6Mb**	**2Ma**	**2Mb**
Al_2O_3	1.63	1.58	1.30	2.14	1.83	2.00	4.78	2.68	4.49	2.66	1.98	2.75	2.23
$Fe_2O_3^t$	4.54	4.52	2.85	6.16	2.11	5.17	10.51	5.64	7.88	5.60	5.60	6.88	5.60
MnO	0.13	0.16	0.41	0.42	0.51	0.52	0.19	0.27	0.13	0.23	0.20	0.20	0.22
P_2O_5	0.059	0.063	0.60	0.76	0.47	0.53	1.40	0.52	0.089	0.17	0.15	0.74	0.56
Cr	68	72	33	62	50	55	134	83	10	106	102	73	71
V	848	880	610	1272	883	1075	2996	1444	90	1744	1395	1342	959
U	6.0	10.2	ND	ND	ND	ND	ND	ND	ND	ND	ND	ND	ND

Table 2: Partial Whole Rock Geochemistry

Sample code	**Sample name**	**δ^{53}Cr (‰)**	**2se**	**Cr/Ti**	**Ti (ppm)**	**V (ppm)**	**Cr (ppm)**
BKA0131	06-2		0.05	0.039	1870	166	73
BKA0132	06-12A	0.97	0.03	0.193	362	1571	70
BKA0133	06-12B	0.76	0.05	0.399	276	1518	110
BKA0134	06-20A	1.38	0.02	0.208	385	1646	80
BKA0135	06-21	0.84	0.04	0.411	74	910	30
BKA0136	06-22	-0.01	0.02	0.003	2043	298	5.5
BKA0137	06-23	0.65	0.03	0.098	570	555	56
BKA0138	06-24	0.64	0.02	0.044	787	156	34
BKA0139	06-30	0.46	0.02	0.051	674	118	34
BKA0140	G-1A	0.66	0.03	0.038	24	10	0.9
BKA0141	G-1B	1.17	0.03	0.036	152	18	5.5
BKA0142	G-2A	0.45	0.02	0.039	76	7.6	3.0
BKA0143	G-2B-A	0.27	0.02	0.060	43	25	2.6
BKA0144	G-2B-B	0.12	0.03	0.071	36	15	2.6
BKA0145	G-3A	0.70	0.02	0.401	225	1212	90
BKA0146	G-3B-X	-0.03	0.02	0.003	1947	112	5.3
BKA0147	G-3B-Y	0.77	0.02	0.248	389	1588	96
BKA0148	CR-1	-0.08	0.03	0.054	34	5.8	1.9
BKA0149	CR-2A	-0.07	0.03	0.047	58	5.3	2.7

Table 3. Cr isotopic data.

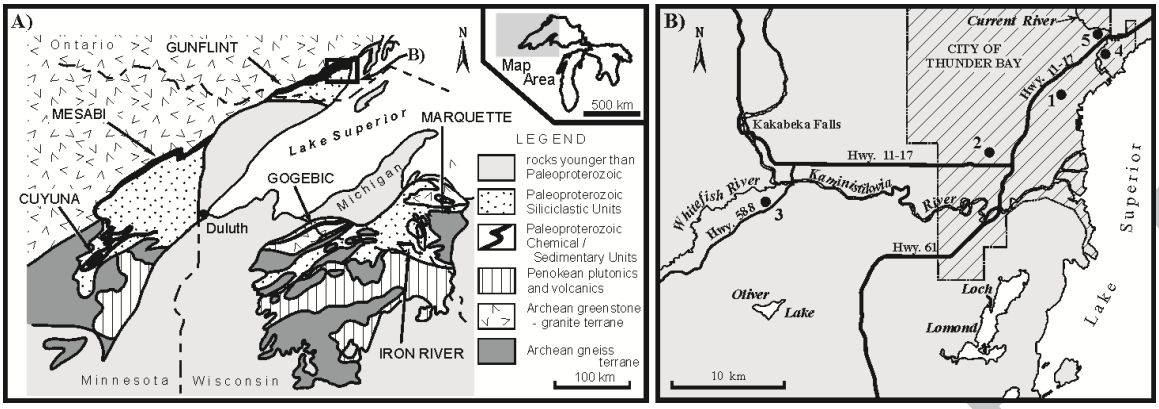

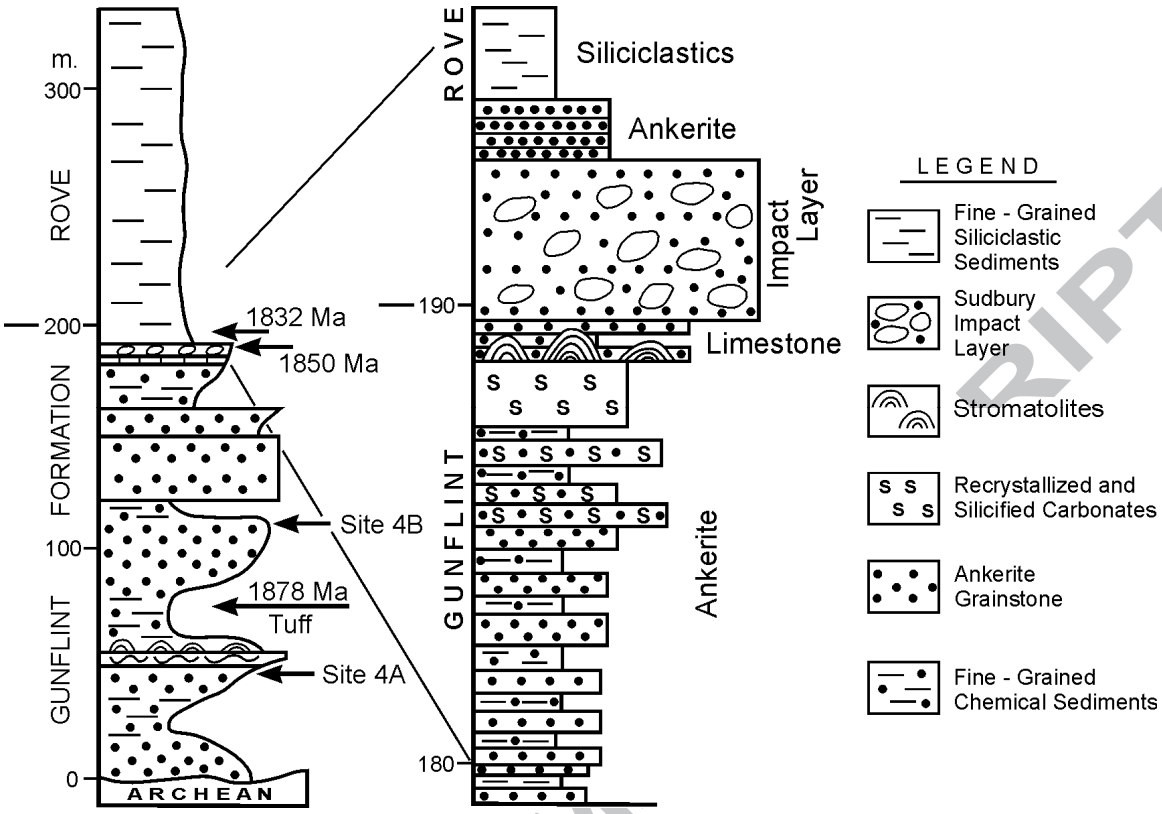

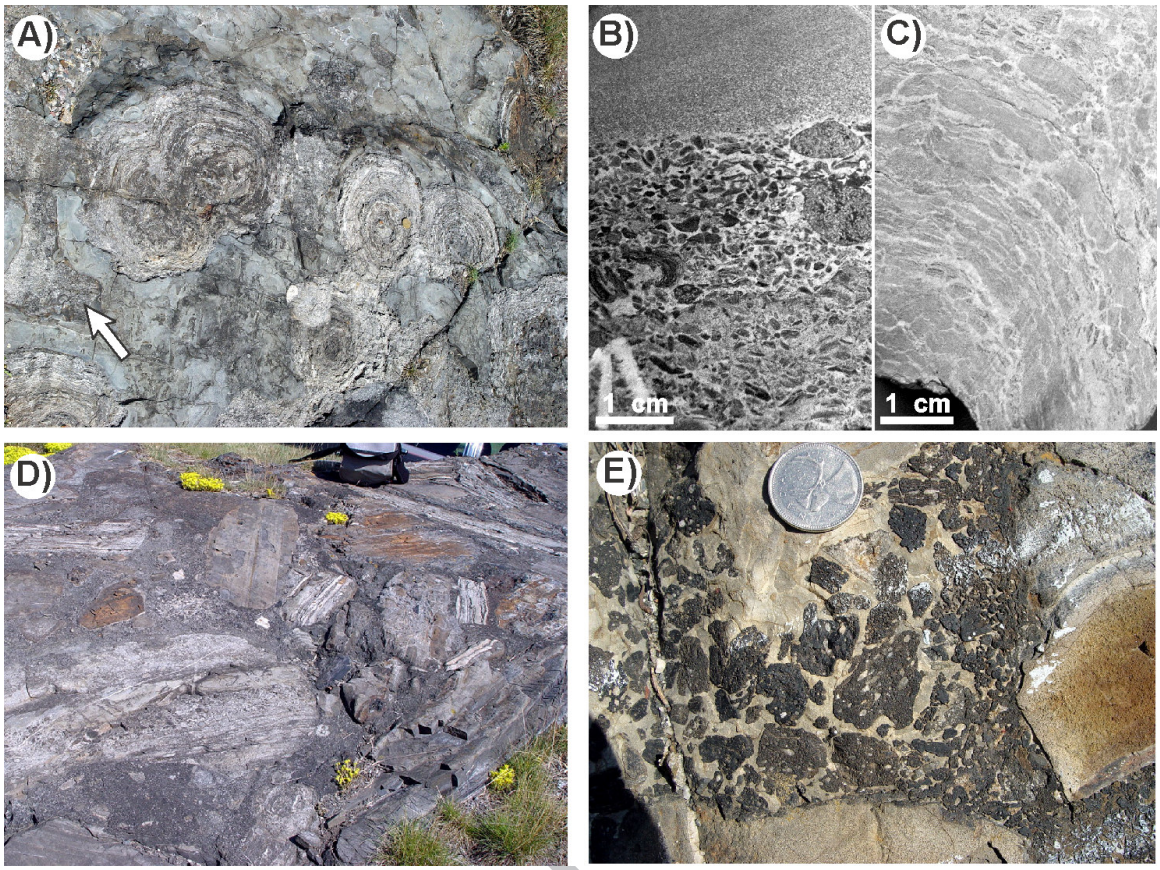

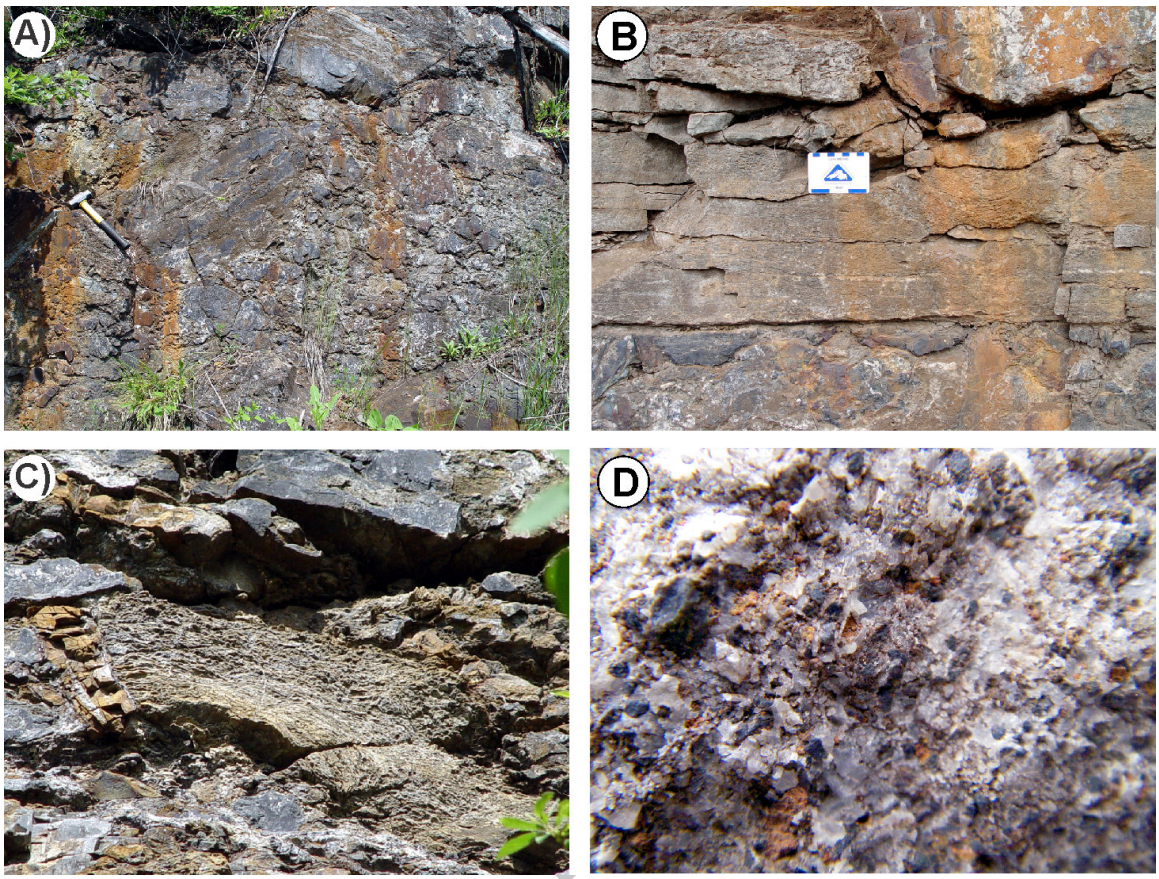

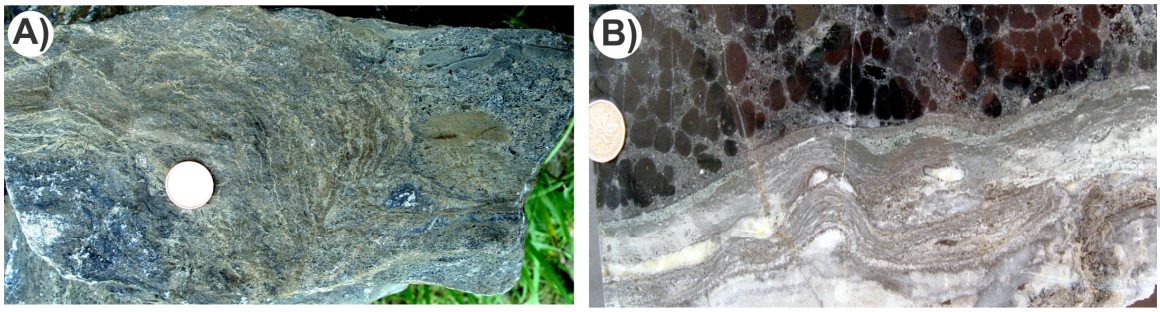

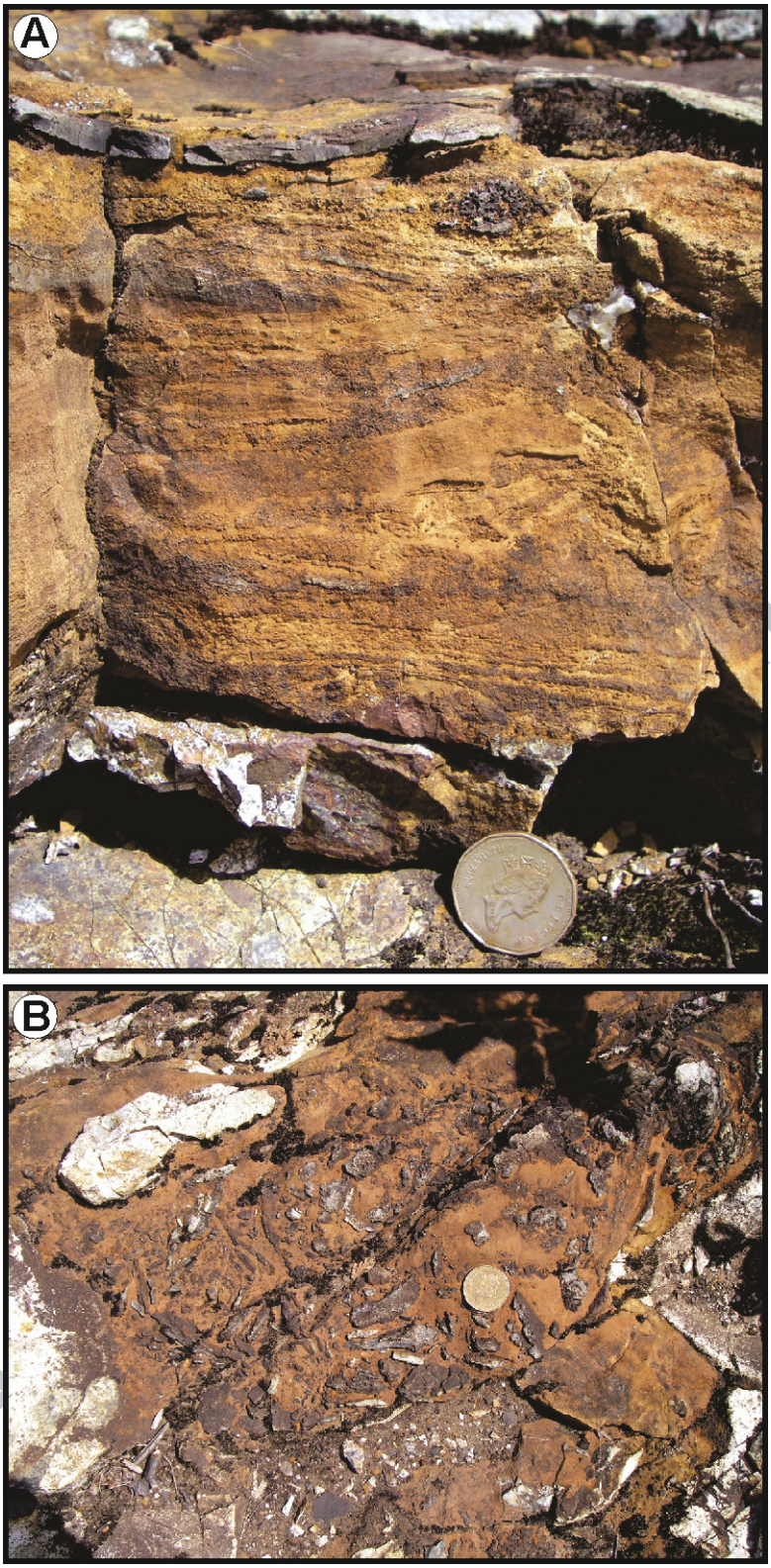

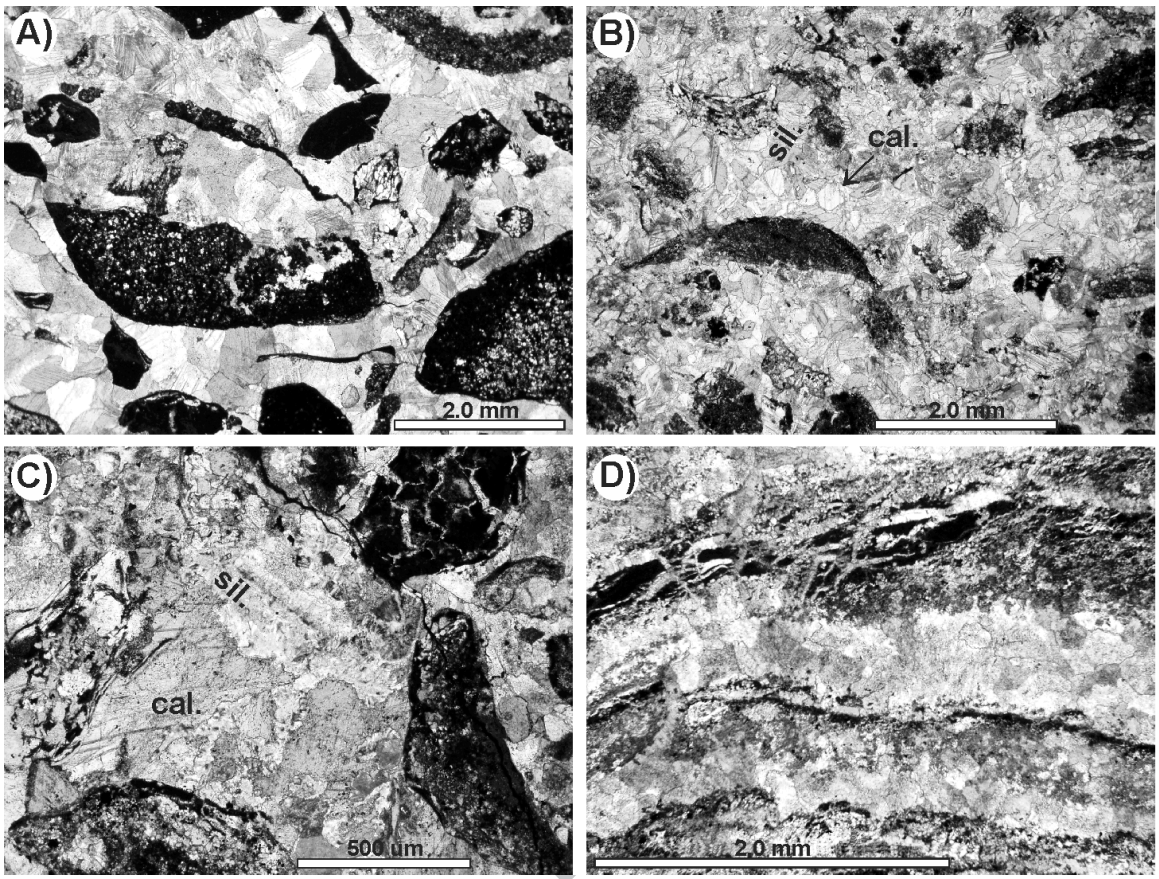

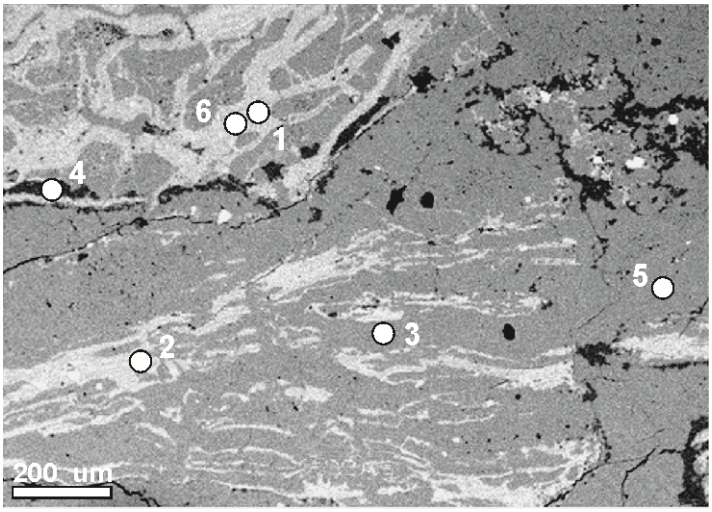

wt. %	1	2	3	4	5	6
SiO_2	25.7	24.8	–	99.0	–	24.5
Al_2O_3	18.5	18.3	–	–	–	19.0
FeO	29.9	30.2	–	–	–	34.4
MgO	9.7	9.4	0.48	–	0.33	6.3
CaO	–	–	50.1	–	52.2	–
MnO	–	–	1.13	–	1.17	–
V_2O_3	1.59	1.56	–	–	–	1.42

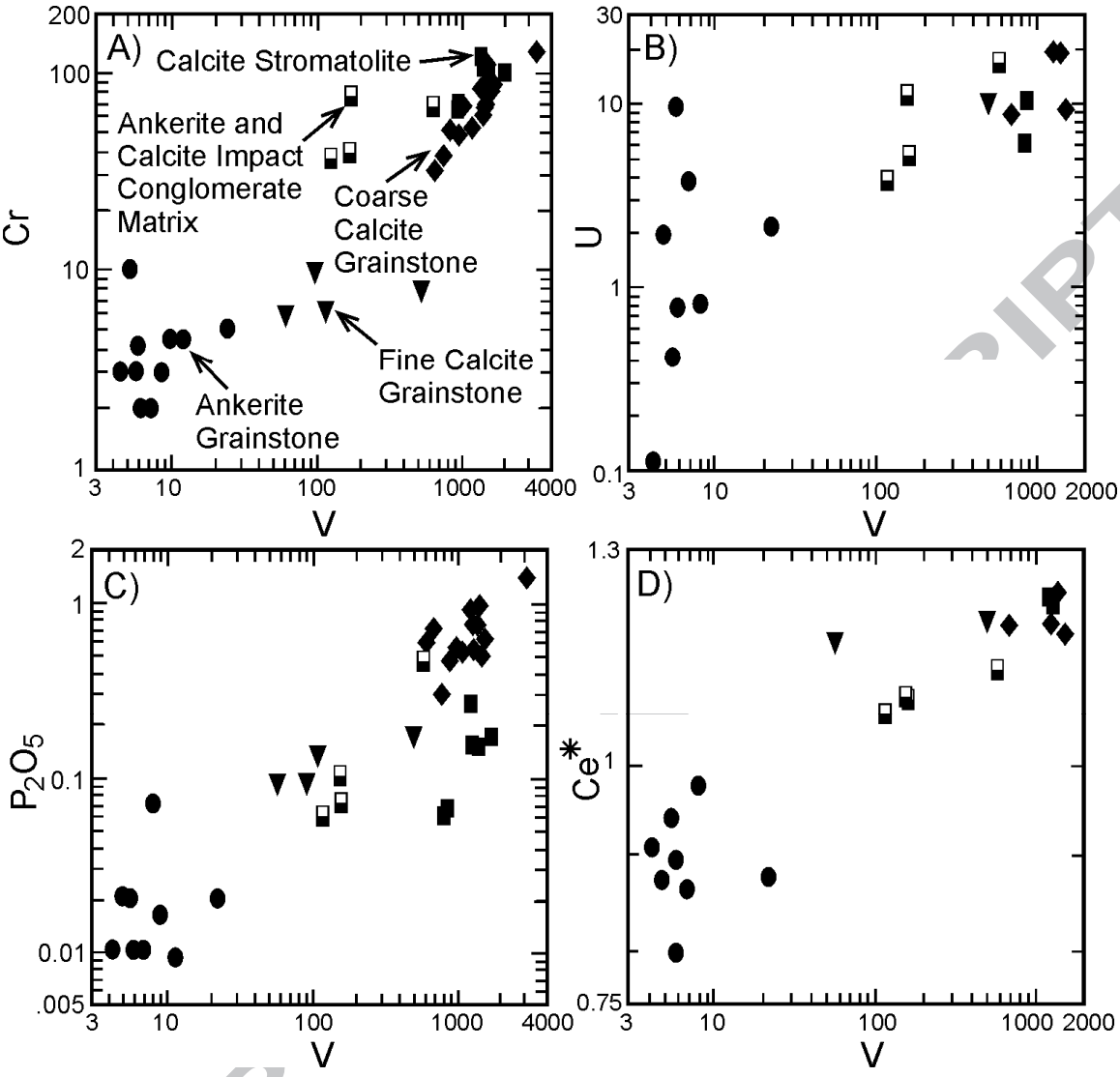

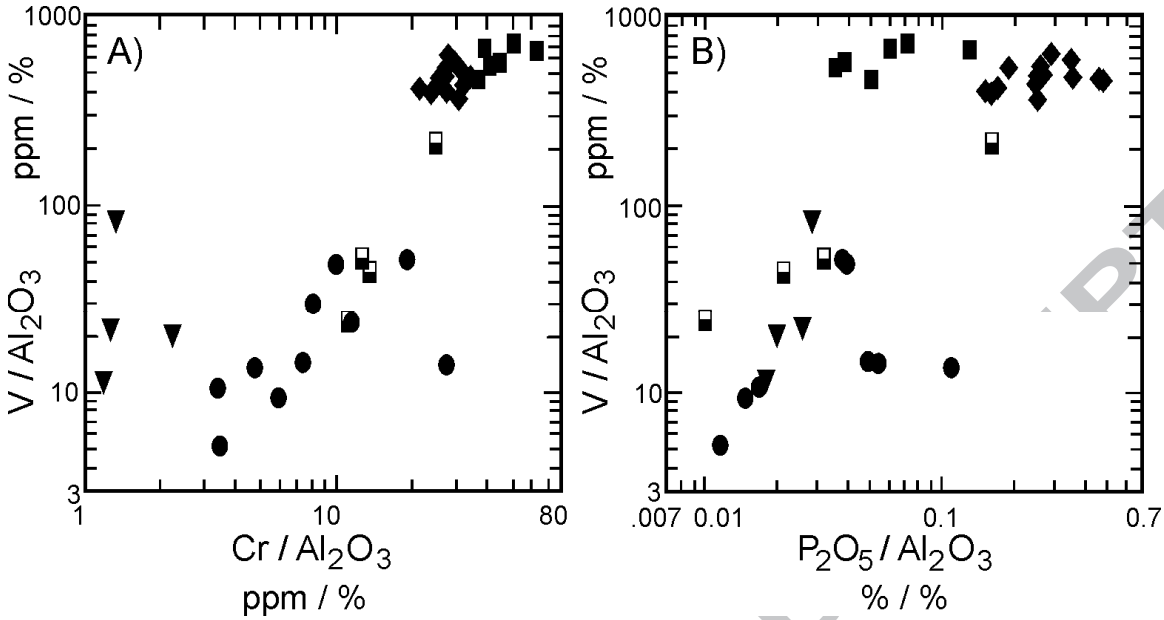

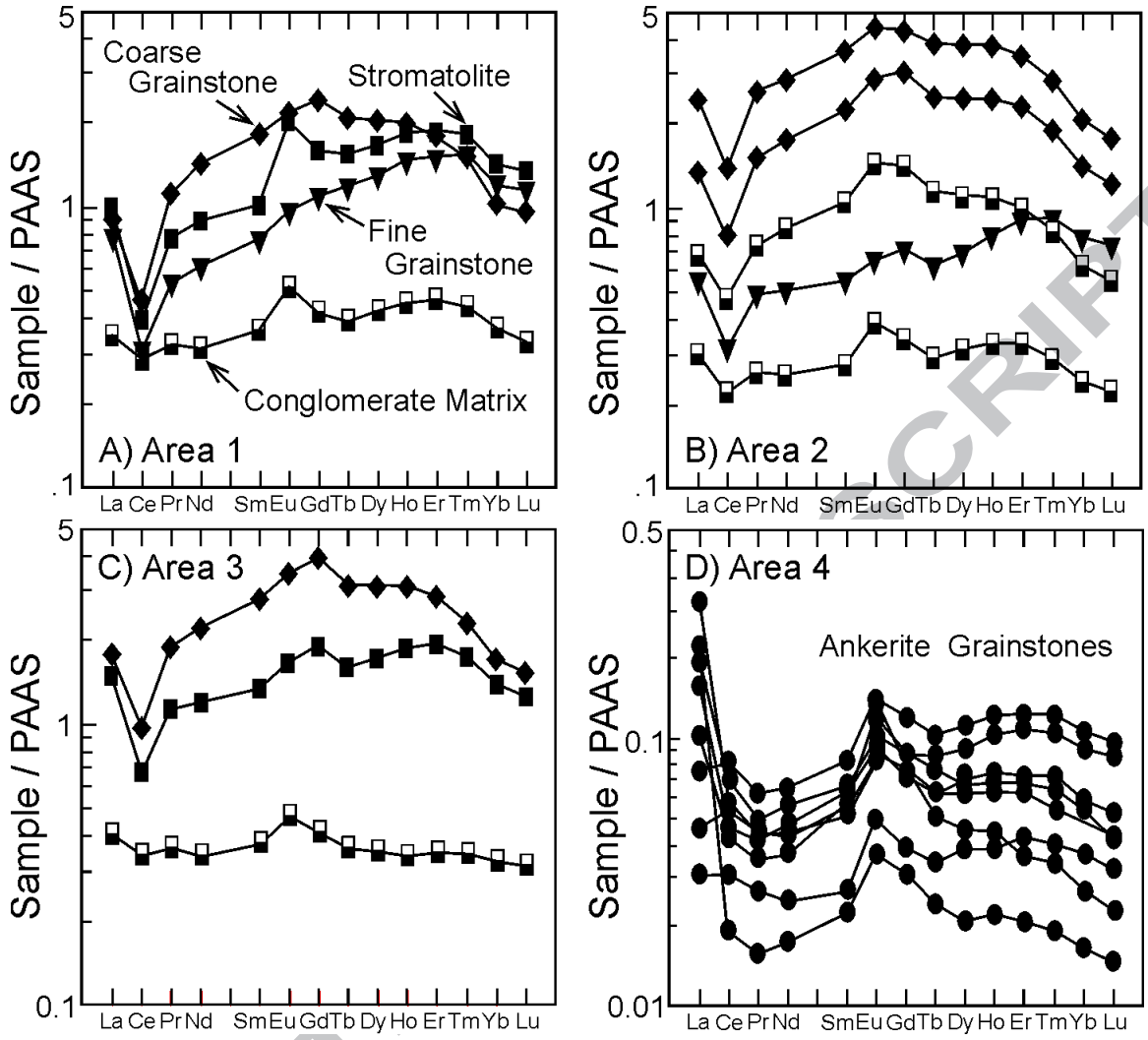

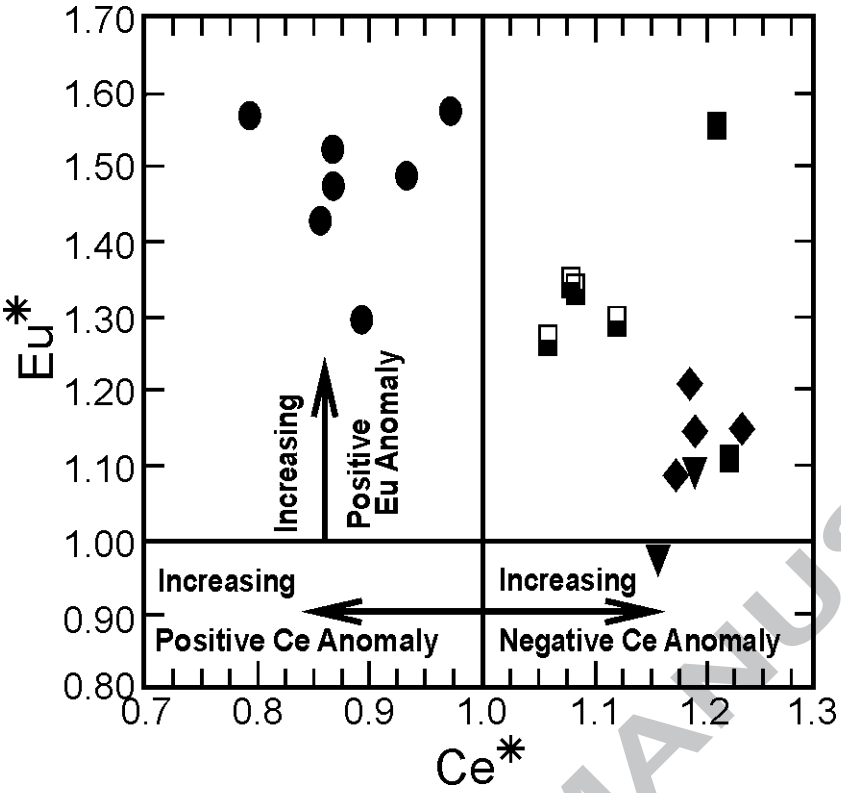

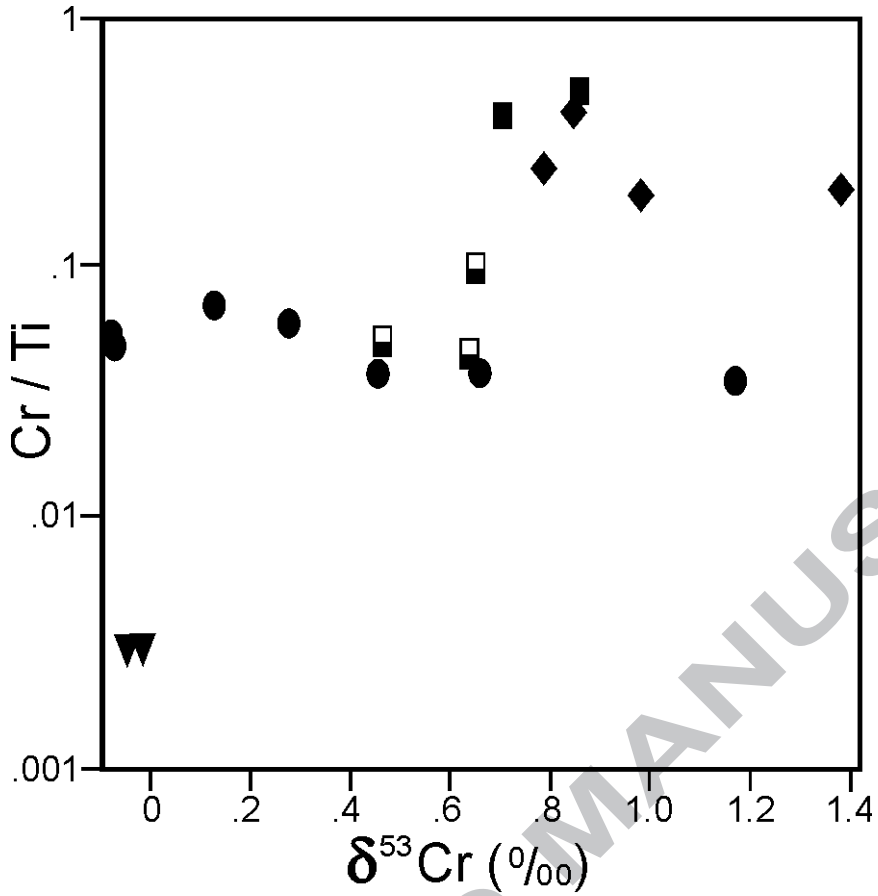

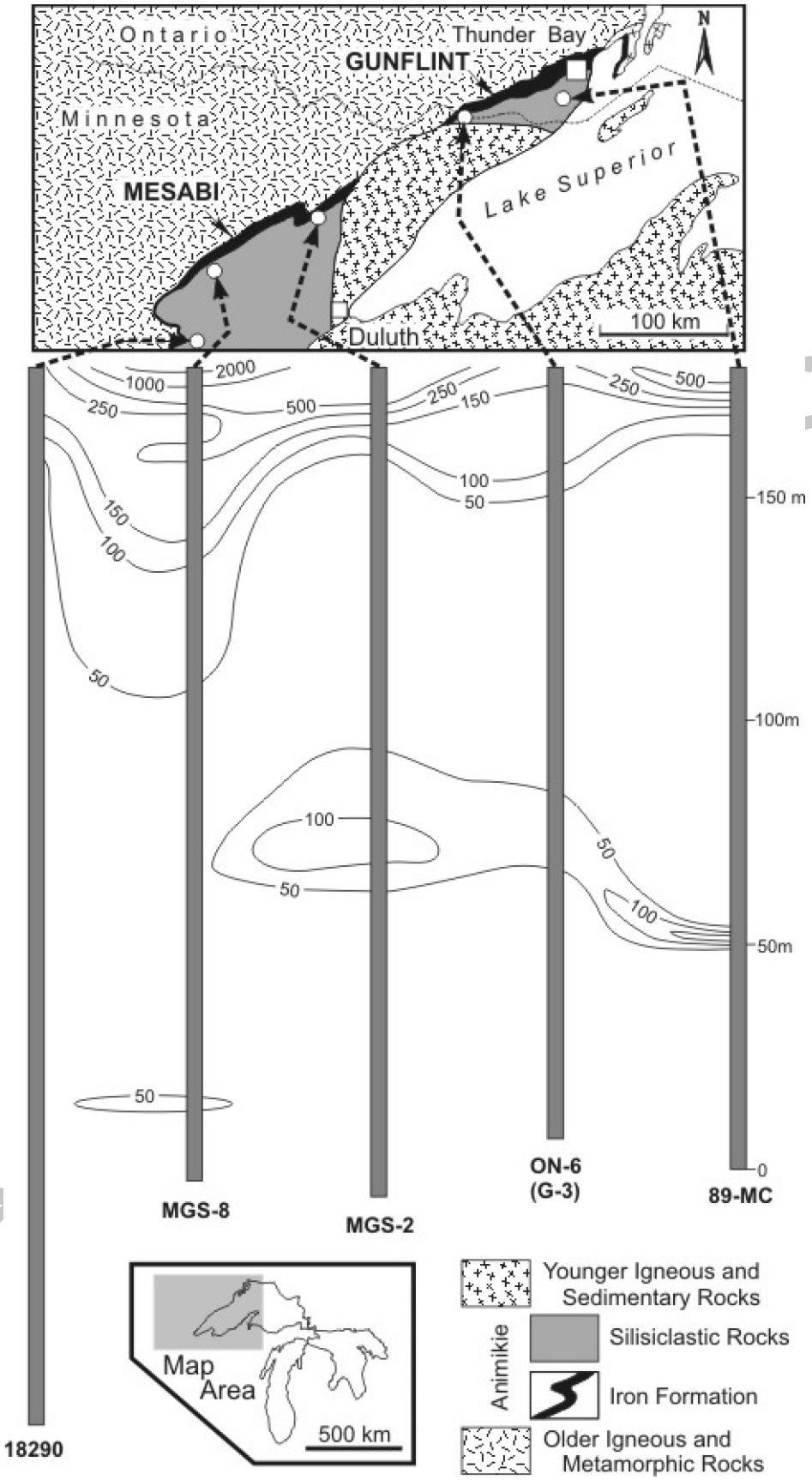

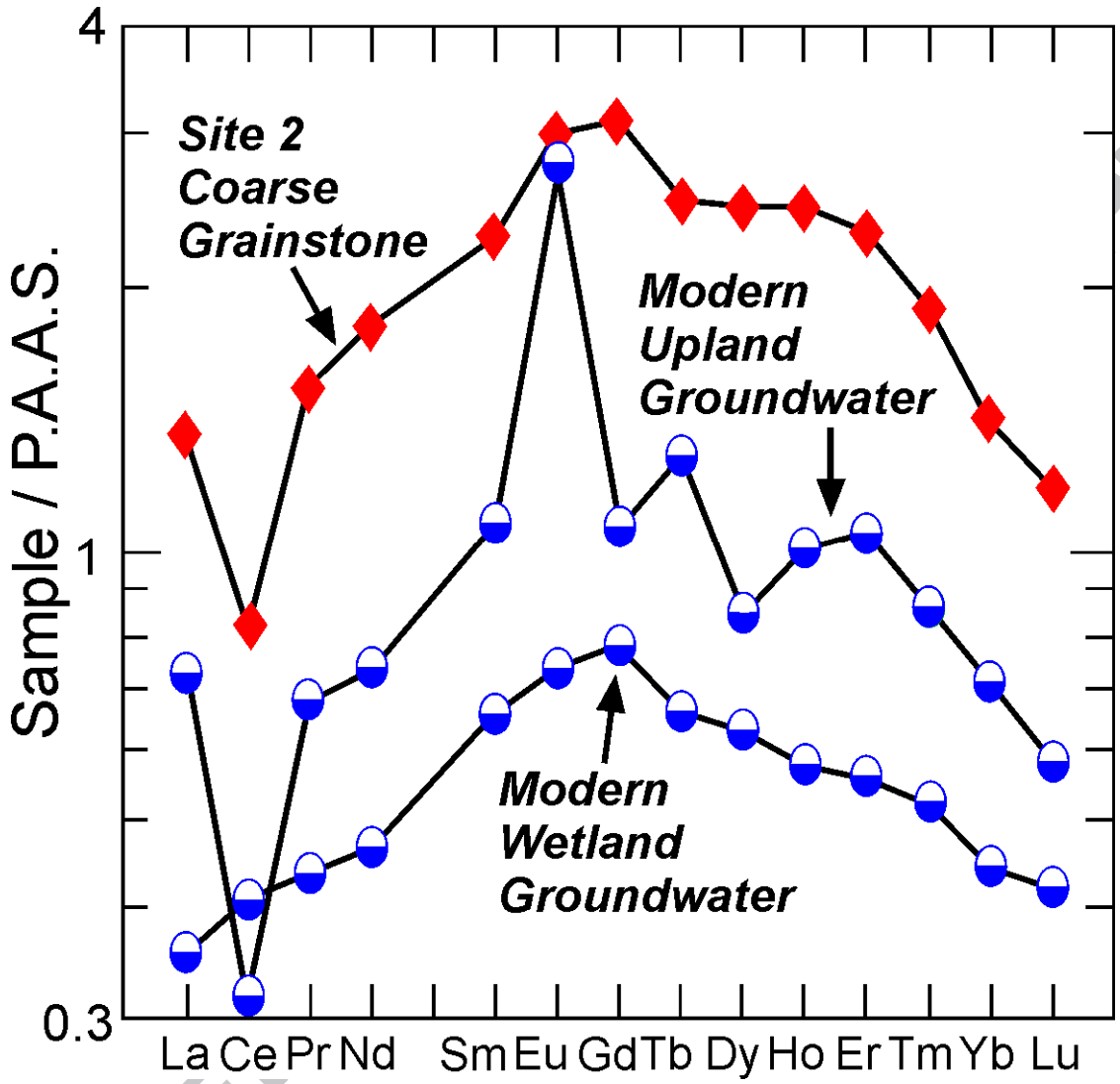

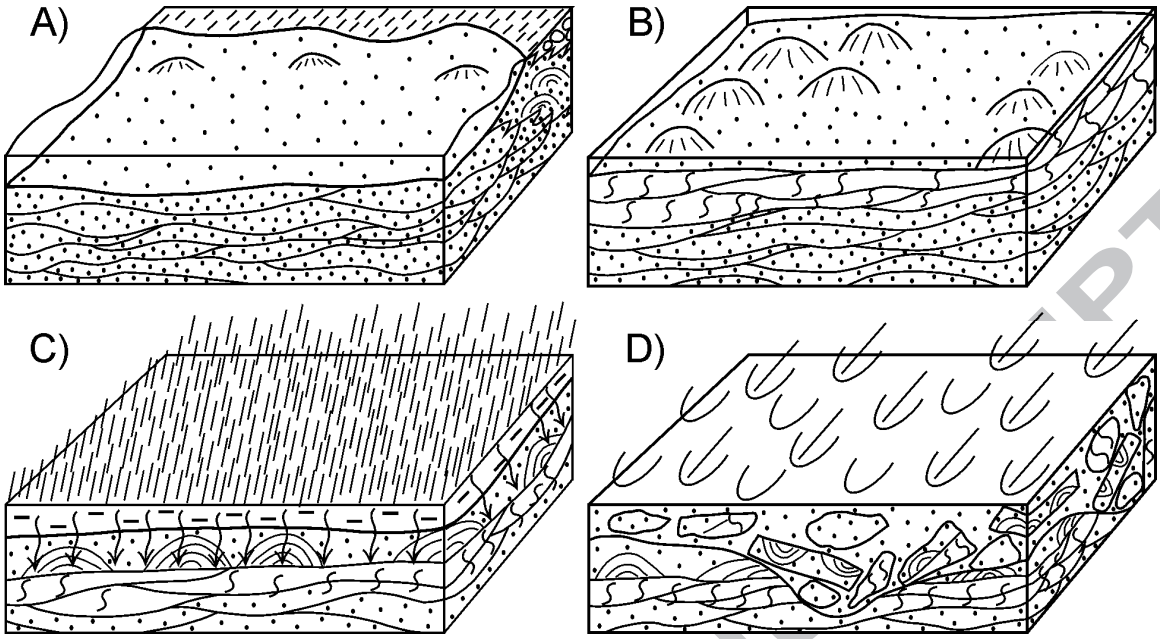

Highlights

The work is important as it utilizes information gained from the Gunflint Formation to outline hitherto unknown atmospheric evolution trends. The Gunflint Formation is one of the most well known rock units in the Precambrian. This notoriety began in the early 50's with the discovery of the first evidence of microfossils in the Precambrian. More recently the Gunflint Formation and overlying Rove Formation have been used by Poulton, Fralick and Canfield (2004 Nature, 2010 Nature Geoscience) to explore the evolution of the hydrosphere-atmosphere geochemical system during this time period. However, a limestone unit at the top of the Gunflint has not been examined in the past, even though these chemical precipitates could provide information on ocean-atmosphere chemistry. This study investigated meteoric cements that formed in this limestone between 1878 and 1850 Ma, and similar meteoric cements that formed in the overlying Sudbury meteoric impact layer between 1850 and 1832 Ma to gain information on atmospheric geochemistry. This is direct evidence of aspects of atmospheric composition as the cements formed sub-aerially. This data is compared to data from Gunflint marine carbonates and shows that the atmosphere had significant oxygen whereas the ocean did not. This may reflect either an imbalance in the ocean-atmosphere system or rapid and profound change in atmospheric oxygen levels. Whichever of these two possibilities is correct will have important ramifications on a great deal of work published in the past on atmosphere-ocean geochemistry in the Precambrian.